MODIS Global Cloud-Top Pressure and Amount Estimation: Algorithm Description and Results

W. PAUL MENZEL, RICHARD A. FREY, HONG ZHANG, DONALD P. WYLIE, CHRIS C. MOELLER, ROBERT E. HOLZ, BRENT MADDUX, BRYAN A. BAUM, KATHY I. STRABALA, AND LIAM E. GUMLEY

Cooperative Institute for Meteorological Satellite Studies, Space Science and Engineering Center, University of Wisconsin—Madison, Madison, Wisconsin

(Manuscript received 29 January 2007, in final form 16 August 2007)

ABSTRACT

The Moderate Resolution Imaging Spectroradiometer (MODIS) on the NASA Earth Observing System (EOS) *Terra* and *Aqua* platforms provides unique measurements for deriving global and regional cloud properties. MODIS has spectral coverage combined with spatial resolution in key atmospheric bands, which is not available on previous imagers and sounders. This increased spectral coverage/spatial resolution, along with improved onboard calibration, enhances the capability for global cloud property retrievals. MODIS operational cloud products are derived globally at spatial resolutions of 5 km (referred to as level-2 products) and are aggregated to a 1° equal-angle grid (referred to as level-3 product), available for daily, 8-day, and monthly time periods. The MODIS cloud algorithm produces cloud-top pressures that are found to be within 50 hPa of lidar determinations in single-layer cloud situations. In multilayer clouds, where the upper-layer cloud is semitransparent, the MODIS cloud pressure is representative of the radiative mean between the two cloud layers. In atmospheres prone to temperature inversions, the MODIS cloud algorithm places the cloud above the inversion and hence is as much as 200 hPa off its true location. The wealth of new information available from the MODIS operational cloud products offers the promise of improved cloud climatologies. This paper 1) describes the cloud-top pressure and amount algorithm that has evolved through collection 5 as experience has been gained with in-flight data from NASA *Terra* and *Aqua* platforms; 2) compares the MODIS cloud-top pressures, converted to cloud-top heights, with similar measurements from airborne and space-based lidars; and 3) introduces global maps of MODIS and High Resolution Infrared Sounder (HIRS) cloud-top products.

1. Introduction

Past estimates of the variation of cloud cover and the earth's outgoing longwave radiation have been derived primarily from the longwave infrared window (10–12 μm) radiances observed from polar-orbiting and geostationary satellites (Rossow and Lacis 1990; Gruber and Chen 1988). The occurrence of semitransparent or cirrus clouds is often underestimated in these single spectral band approaches; cirrus allow solar heating while reducing infrared radiation to space, and thus are crucially important to global radiative processes and the energy balance of the earth. Models of climate changes will have to correctly simulate these clouds to have the proper radiative terms for the earth's heat budget; however, clouds remain the largest uncertainty in climate model forecasts (Stephens 2005). Multispectral techniques have been used to better detect cirrus in global (Wylie et al. 2005; Wu and Susskind 1990) cloud studies, but at spatial resolutions of tens of kilometers. The Moderate Resolution Imaging Spectroradiometer (MODIS) offers the opportunity to investigate seasonal and annual changes in the cirrus or semitransparent global cloud cover and cloud phase with multispectral observations at high spatial resolution (1 km). Transmissive clouds that are partially transparent to terrestrial radiation can be reliably separated from opaque clouds in the statistics of cloud cover (Wylie and Menzel 1989). This paper describes the MODIS cloud-top pressure and amount algorithm applied to 5-km areas and presents some global examples along with validating observations. Major features introduced in the ap-

Corresponding author address: W. Paul Menzel, UW-CIMSS, 1225 W. Dayton St., Madison, WI 53706.
E-mail: paul.menzel@ssec.wisc.edu

DOI: 10.1175/2007JAMC1705.1

TABLE 1. *Terra* MODIS spectral bands used in the cloud-top pressure and amount algorithm, including bandwidths, principal absorbing components, and approximate pressure level corresponding to the peak in the individual band-weighting functions.

MODIS band No.	MODIS bandwidth (μm)	Principal absorbing components	Approximate peak in weighting function (hPa)
31	10.8–11.3	H_2O, CO_2	Surface
32	11.8–12.3	H_2O, CO_2	Surface
33	13.2–13.5	H_2O, CO_2, O_3	900
34	13.5–13.8	H_2O, CO_2, O_3	700
35	13.8–14.1	H_2O, CO_2, O_3	500
36	14.1–14.4	H_2O, CO_2, O_3, N_2O	300

plication of the algorithm to MODIS data include 1) using the 1-km cloud mask to indicate what part of a 5-km area is cloudy, 2) implementing a radiance bias correction for calculated and observed clear-sky radiances, and 3) identifying cloud types (thin, thick, and opaque) in the level-3 aggregation of cloud cover.

2. Instrument characterization and preprocessing

a. MODIS

MODIS is a 36-band whisk-broom-scanning radiometer currently flying on the National Aeronautics and Space Administration (NASA) *Terra* and *Aqua* platforms. *Terra* was launched in December 1999 into a (daytime) descending orbit with an equatorial crossing of 1030 local solar time (LT). *Aqua,* launched in May 2002, is in an ascending orbit with a 1330 LT crossing time. MODIS has four focal planes that cover the spectral range from 0.42 to 14.24 μm, with each spectral band defined by an interference filter. Spatial resolution at nadir varies from 250 m to 1 km, depending on the spectral band. MODIS has several onboard instruments for in-orbit radiometric and spectral characterization. A solar diffuser panel is used for reflectance calibration for bands with wavelengths from 0.45 through 2.1 μm, and an accompanying diffuser stability monitor is used to assess the stability of the diffuser at wavelengths up to 1 μm. Thermal spectral bands are calibrated with an onboard blackbody. The MODIS bands used in the cloud-top pressure and amount algorithm are presented in Table 1.

b. Ongoing instrument characterization

As with any retrieval method, the quality of the products depends critically on accurate characterization and calibration of the MODIS level-1B (L1B) radiance data. The data from both the *Terra* and *Aqua* imagers have required in-depth analyses to characterize the instrument behavior. In particular, for the cloud-top property determinations, there were significant challenges in mitigating performance issues raised by long-wavelength infrared (LWIR) band cross talk, scan-mirror reflectance variation with scan angle, and detector striping.

Prelaunch testing of the MODIS protoflight model on *Terra* revealed a light leak from the infrared window (band 31, 11 μm) into bands 32–36 (wavelengths ranging from 12 to 14.3 μm). The leak included both spatial and spectral components. The radiometric impacts for typical radiances in these bands ranged from less than 1% in band 32 to more than 10% in band 36; these are near or exceed the radiometric accuracy specification of 0.5% (band 32) and 1% (bands 33–36) at typical scene temperatures. A linear correction algorithm was developed to reduce the contamination in these bands.

Terra MODIS scan-mirror response-versus-scan-angle (RVS) characterization was not measured at the system level in prelaunch tests; after launch an unexpectedly large asymmetry was found in the LWIR bands. There was a significant difference in the radiances from one side of the scan to the other; this led to systematic biases in several cloud products as a function of scan angle. A *Terra* deep-space maneuver, performed in 2003, enabled a high-quality RVS characterization that was applied to the operational level-1B processing algorithm. This effectively removed the cross-track asymmetry in the LWIR bands.

A detector destriping algorithm for MODIS level-1B 1-km image data, based on Weinreb et al. (1989), has been used to mitigate the effects of detector-to-detector and mirror-side differences. MODIS LWIR measurements are accomplished with 20 detector–mirror-side combinations (10 detectors on each mirror side); each represents 20 different calibrations potentially contributing to striping. An empirical distribution function (EDF) is computed for each detector–mirror combination (also known as the cumulative histogram of relative frequency). The EDF for each detector–mirror is then adjusted to match the EDF of a reference detector–mirror. Calibration is maintained through the reference detector. This destriping process is currently performed for each MODIS granule.

Moeller et al. (2003) describe the verification of the radiometric integrity of MODIS measurements and report that calibration correction algorithms are producing performance within specification for most of the infrared bands. As calibration issues have been addressed, adjustments have been incorporated into the MODIS L1B production code for use in the current generation (known as a "collection") of MODIS L1B radiances and level-2 science products. Each collection includes reprocessing of historical MODIS data and forward processing of the ongoing measurements, until the beginning of the next collection. Each collection uses the best-available postlaunch instrument characterization, as well as science product algorithm adjustments, including improved treatment of surface emissivity and skin temperature, mitigation of day–night science product biases, and improved efficiency in production code.

The algorithms and examples of early MODIS cloud products data are presented in Platnick et al. (2003) and King et al. (2003). With careful and continual evaluation of the instrument and cloud products, recent collections (production runs) are of a much higher quality than earlier versions. Up-to-date information on *Terra* and *Aqua* algorithm versions and reprocessing efforts are given on the MODIS atmosphere group Web site (online at http://modis-atmos.gsfc.nasa.gov/products_calendar.html).

c. MODIS cloud product generation

The MODIS cloud products are generated on a granule basis; a granule consists of 5 min of data aggregated in units of 10 along-track pixels (usually 2030, but occasionally 2040). Cloud-top pressure and effective cloud amount are generated at 5-km resolution (processing 5×5 pixels in the granule) from the average of the cloudy pixel radiances within the 5-km area, using the cloud mask to identify cloudy pixels. These cloud products are archived in a single Hierarchical Data Format (HDF) file with MOD06 (*Terra*) and MYD06 (*Aqua*) product designation; similarly, the cloud mask is found in MOD35 and MYD35.

After the level-2 granule-level cloud products have been produced globally, spatial and temporal composites are aggregated to daily, 8-day, and monthly data. Statistics are sorted onto a $1^\circ \times 1^\circ$ equal-angle grid containing 180×360 individual cells. The level-3 atmosphere product is derived separately for *Terra* (MOD08) and *Aqua* (MYD08). For the daily product, every level-2 granule that overlaps any part of the data day, defined as being from 0000 to 0000 UTC next day, is included in the compositing process. A granule that spans either 0000 or 0000 UTC next day may be included in two consecutive MOD08 daily products. The 8-day product is derived from the daily level-3 products collected over eight consecutive days. The 8-day intervals are reset at the beginning of each year in concert with the level-3 products produced by the MODIS ocean and land discipline groups. The monthly product provides a summary of the daily products obtained over a calendar month.

While there is no separation of the cloud parameters by ascending or descending node, there is a day–night separation. Daytime is specified by a solar zenith angle of less than 85°. Cloud fractions (from the cloud mask) and cloud-top pressures are processed for both day and night and are provided in the level-3 products as daytime only, nighttime only, and combined day and night.

3. Cloud-top pressure algorithm

MODIS cloud-top pressure and effective cloud amount (i.e., cloud fraction multiplied by cloud emissivity) are determined using radiances measured in spectral bands located within the broad 15-μm CO_2 absorption region. The CO_2-slicing technique is based on the atmosphere becoming more opaque resulting from CO_2 absorption as the wavelength increases from 13.3 to 15 μm, thereby causing radiances obtained from these spectral bands to be sensitive to a different layer in the atmosphere. The CO_2-slicing approach has a long history, having been applied to data from both the High Resolution Infrared Radiometer Sounder (HIRS; Wylie and Menzel 1999) and the Geostationary Operational Environmental Satellite (GOES) sounder (Menzel et al. 1992; Menzel and Purdom 1994). Error analyses for the method are provided in Menzel et al. (1992) and Baum and Wielicki (1994). The historical record of cloud properties from sounder data spans more than 25 yr. MODIS provides measurements at 1-km resolution in four wavelengths located within the 15-μm CO_2 band. MODIS cloud-top properties (CTPs; e.g., cloud-top pressure and effective cloud amount) are produced for the cloudy portion of the 5×5 pixel arrays wherein the radiances for the cloudy pixels (as designated by the 1-km-resolution cloud mask) are averaged to reduce radiometric noise. Thus, the CTP is produced at 5-km spatial resolution in collection 5. It is a goal to generate CTP at both 1- and 5-km resolution in the next collection.

The MODIS cloud-top pressure is converted to cloud height and cloud temperature through the National Centers for Environmental Prediction (NCEP) Global Forecast System (GFS; Derber et al. 1991), which provides gridded temperature profiles at 25-hPa intervals

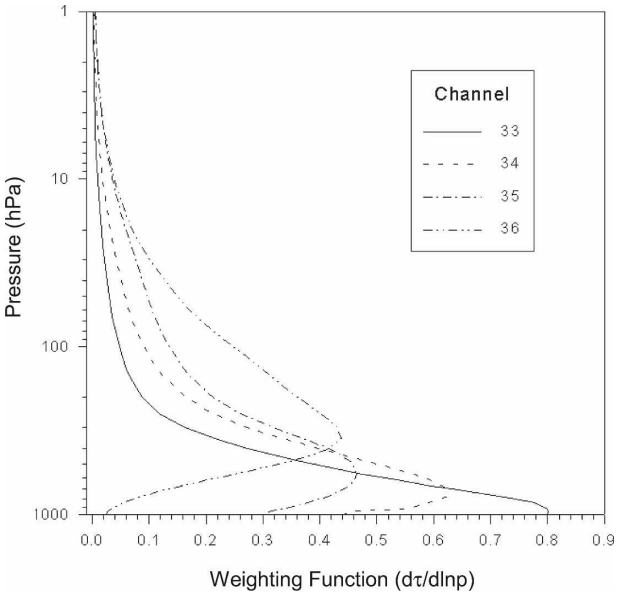

FIG. 1. Weighting functions for the four MODIS bands in the CO_2 absorption band.

from 1000 to 900 hPa; 50-hPa intervals from 900 to 100 hPa; and at 70, 50, 30, 20, and 10 hPa every 6 h. Differences between model-derived and measured clear-sky radiances are mitigated with a radiance bias adjustment to avoid height assignment errors. Cloud properties are derived in the same way for both day- and nighttime data because the IR method is independent of solar illumination.

Figure 1 shows the weighting functions for the CO_2 absorption bands on MODIS. Because the peaks in the weighting functions are well into the troposphere, CO_2 slicing is most effective for the analysis of mid- to high-level clouds, especially semitransparent clouds such as cirrus. Use of the 15-μm bands is constrained when the cloud signal (change in radiance caused by the presence of cloud) becomes comparable to instrument noise, as in optically thin clouds and clouds occurring in the lowest 3 km of the atmosphere. When low clouds are present, the 11-μm infrared window brightness temperature data are used to estimate an opaque cloud-top temperature, and then pressure (or height) is inferred by comparison with a model analysis working from the tropopause downward; in the case of low-level temperature inversions, the pressure of the matching temperature above the inversion is selected. In the MODIS cloud properties algorithm, a great majority of low-level cloud pressure altitudes are derived from the 11-μm infrared window data rather than the CO_2-slicing data; this is due to the small signal seen in radiances measured in the 15-μm CO_2 absorption band that emanate from clouds below about 700 hPa.

The CO_2-slicing technique is founded in the calculation of radiative transfer in an atmosphere with a single cloud layer. For a given cloud element in a field of view (FOV), the radiance observed $R(\upsilon)$ in spectral band υ can be written as

$$R(\upsilon) = (1 - NE)R_{\mathrm{clr}}(\upsilon) + NE[R_{\mathrm{bcd}}(\upsilon, P_c)], \quad (1)$$

where $R_{\mathrm{clr}}(\upsilon)$ is the clear-sky radiance, $R_{\mathrm{bcd}}(\upsilon, P_c)$ is the opaque (black) cloud radiance from pressure level P_c, N is the fraction of the field of view covered with cloud, and E is the cloud emissivity. It is apparent from this expression that if the emissivity is overestimated, then the cloud-top pressure will also be overestimated (thereby putting the cloud too low in the atmosphere).

The opaque (black) cloud radiance can be calculated from

$$R_{\mathrm{bcd}}(\upsilon, P_c) = R_{\mathrm{clr}}(\upsilon) - \int_{P_c}^{P_s} \tau(\upsilon, p)\frac{dB[\upsilon, T(p)]}{dp}\,dp, \quad (2)$$

where P_s is the surface pressure, P_c is the cloud pressure, $\tau(\upsilon, p)$ is the fractional transmittance of radiation at frequency υ emitted from the atmospheric pressure level (p) arriving at the top of the atmosphere ($p = 0$), and $B[\upsilon, T(p)]$ is the Planck radiance at frequency υ for temperature $T(p)$. The second term on the right represents the decrease in radiation from clear conditions introduced by the opaque cloud.

The inference of cloud-top pressure for a given cloud element is derived from radiance ratios between two spectral bands following the work of Smith and Platt (1978). The ratio of the deviations in observed radiances $R(\upsilon)$ to their corresponding clear-sky radiances $R_{\mathrm{clr}}(\upsilon)$ for two spectral bands of wavenumber υ_1 and υ_2, viewing the same FOV, is written as

$$\frac{R(\upsilon_1) - R_{\mathrm{clr}}(\upsilon_1)}{R(\upsilon_2) - R_{\mathrm{clr}}(\upsilon_2)} = \frac{NE_1\displaystyle\int_{P_s}^{P_c} \tau(\upsilon_1, p)\frac{dB[\upsilon_1, T(p)]}{dp}\,dp}{NE_2\displaystyle\int_{P_s}^{P_c} \tau(\upsilon_2, p)\frac{dB[\upsilon_2, T(p)]}{dp}\,dp}. \quad (3)$$

For frequencies that are spaced closely in wavenumber, the assumption is made that E_1 is approximately equal to E_2. This allows the pressure of the cloud within the FOV to be specified when the atmospheric temperature and transmittance profiles for the two spectral bands are known or estimated.

Once a cloud-top pressure has been determined, an effective cloud amount (also referred to as effective

emissivity) can be evaluated from the infrared window band data using the relation

$$NE = \frac{R(w) - R_{\mathrm{clr}}(w)}{B[w, T(P_c)] - R_{\mathrm{clr}}(w)}. \quad (4)$$

Here NE is the effective cloud amount, w represents the window band frequency, and $B[w, T(P_c)]$ is the opaque cloud radiance. The effective cloud amount cannot be calculated without an estimate of the window band (11 μm) clear-sky radiance. When NE is less than unity, MODIS may be observing broken opaque cloud ($N < 1$, $E = 1$), overcast transmissive cloud ($N = 1$, $E < 1$), or broken transmissive cloud ($N < 1$, $E < 1$). When viewing mid- to high-level clouds with an observational area of roughly 5-km resolution, the semitransparency for a given field of view is more often due to cloud emissivity being less than one than the cloud not completely covering the field of view. Wylie et al. (1994) found this to be true for most synoptic regimes, especially in the tropics and subtropics.

Equation (3) is used to estimate the mean cloud properties within a 5 km $\times$ 5 km area. On the left side of Eq. (3), cloud radiances are determined by averaging only the radiances for those 1-km pixels designated to be probably cloudy or cloudy by the cloud mask (at least four must be flagged); this enables enhancement of the signal-to-noise ratio. Clear-sky radiances for each MODIS band are estimated in a radiative transfer calculation of the MODIS spectral band radiances using a transmittance model called the Pressure Layer Fast Algorithm for Atmospheric Transmittances (PFAAST; Hannon et al. 1996); this model has 101 pressure-level vertical coordinates from 0.05 to 1100 hPa. The calculations account for the satellite viewing angle, absorption by well-mixed gases (including nitrogen, oxygen, and carbon dioxide), water vapor (including the water vapor continuum), and ozone. The global analyses of temperature and moisture fields from the NCEP GFS and Reynolds-blended sea surface temperatures (Reynolds and Smith 1994) are used to define the fields of temperature and moisture used in the forward calculation.

The right side of Eq. (3) is calculated from the GFS temperature and moisture profile and the PFAAST profiles of atmospheric transmittance for the spectral bands as a function of P_c, the cloud-top pressure. The integration through the atmosphere is accomplished at discrete intervals, and the inferred cloud-top pressure is rounded to the nearest 5 hPa. A radiance bias adjustment of measured versus GFS-calculated clear-sky radiances is incorporated based on the previous 8-day clear-sky radiance composite; this adjustment is necessary to assure that the right and left sides of Eq. (3) are balanced.

With the assumption that the emissivity of the clouds is the same for the two spectral bands, the P_c that best matches measured and calculated ratios is deemed a candidate solution for the cloud-top pressure; the search is restricted between the surface pressure (or the top of the inversion layer) and the tropopause.

The cloud-top pressure is selected with a "top-down" approach. If the two most opaque bands (e.g., 14.24 and 13.94 μm) detect cloud so that ($R - R_{\mathrm{clr}}$) for both bands is greater than the instrument noise [conservatively estimated at 1 mW m^{-2} (sr cm^{-1})$^{-1}$] and Eq. (3) produces a solution high in the troposphere, this is taken as the cloud-top pressure solution and no other band ratios are investigated. This ratio is most sensitive to the highest clouds. If the most opaque bands do not produce a solution, a ratio of less opaque bands (e.g., 13.94/13.64 μm) is investigated for a solution in the upper part of the troposphere; if found, this is taken as the cloud-top pressure solution and no other bands are investigated. This ratio is generally more sensitive to midlevel clouds and cloud edges where information from the atmosphere below the cloud is important. If the less opaque bands do not produce a solution, a ratio of even less opaque bands (e.g., 13.64/13.34 μm) is investigated. This would yield the cloud-top pressure for the lowest-level clouds.

Thus, for *Aqua* MODIS, ratios 36/35, 35/34, and 34/33 are used (14.24/13.94 μm, 13.94/13.64 μm, and 13.64/13.34 μm, respectively). Because *Terra* MODIS has severe noise problems in band 34, only ratios 36/35 and 35/33 are used.

If N_c is the number of cloudy pixels within the 5 km $\times$ 5 km area [estimated using the cloud mask of Ackerman et al. (1998)], then the representative effective cloud amount for the 5-km area will be the NE determined for the cloudy pixels adjusted to represent all the pixels in the 5 $\times$ 5 pixel array [e.g., $NE_{5\times5} = N_c NE/25$)]. The cloud-top temperature is recorded as the value indicated by the GFS temperature profile at the level specified by the cloud-top pressure retrieval.

If a radiance ratio cannot be calculated reliably for any of the possible spectral band pairs because ($R - R_{\mathrm{clr}}$) is within the instrument noise level, then a cloud-top pressure is calculated directly from the infrared window band, assuming it has an adequate signal-to-noise ratio. The observed 11-μm infrared window band brightness temperature is used to infer a cloud-top pressure by comparison with an 11-μm brightness temperature profile derived from the gridded GFS product (using a radiative transfer calculation for all possible opaque cloud-top pressures that includes water vapor

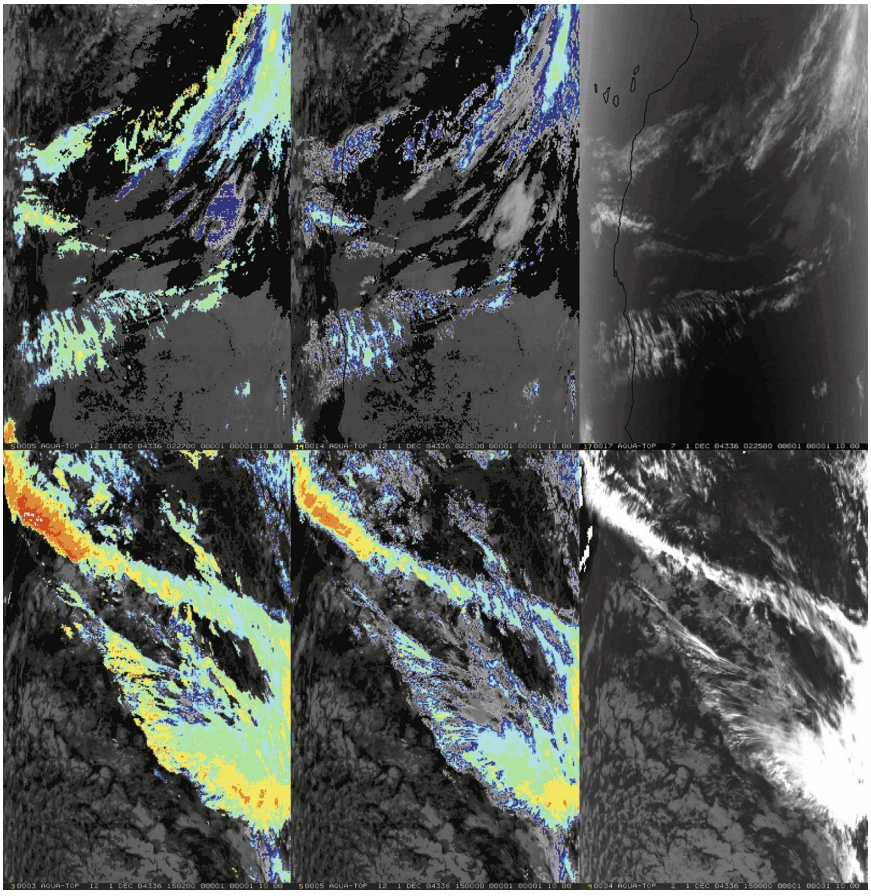

FIG. 2. *Aqua* MODIS CTP results (CTP < 400 in color) for two different scenes on 1 Dec 2004 (left) after radiance bias adjustment and (middle) before radiance bias adjustment, and (right) a black and white infrared image of the scene. Clouds between 95 and 125 hPa (white), 125 and 160 hPa (red), 160 and 190 hPa (orange), 190 and 225 hPa (yellow), 225 and 260 hPa (aqua), 260 and 300 hPa (cyan), 300 and 330 hPa (sky), 330 and 360 hPa (blue), and 360 and 390 hPa (navy) are shown.

attenuation above the cloud); the cloud emissivity is assumed to be unity and $NE = N_c/25$. In this way, all clouds are assigned a cloud-top pressure either by CO_2 or LWIR window calculations. Optically thin, high clouds are sometimes mistaken for low-level opaque clouds; Wylie and Menzel (1989) found that this occurred for about half of the very thin clouds with *NE* less than 10%.

In summary, the calibrated and navigated MODIS data are processed for 5 × 5 pixel areas. Single pixels are determined to be clear or cloudy from the cloud mask. Cloud properties are calculated for the cloudy pixels in the 5 × 5 pixel area. In the case where 22–25 of the 1-km pixels are clear, no cloud parameters are calculated. The data are corrected for satellite viewing angle to minimize the impact of the increased pathlength through the atmosphere of radiation upwelling to the satellite. Global coverage is realized every 2 days with one satellite.

4. Algorithm considerations

The accuracy of the cloud retrieval depends on good calibration, knowledge of spectral response functions, atmospheric characterization, accurate and computationally fast radiative transfer models to simulate top-of-atmosphere radiances, and a reliable cloud mask. For the *Aqua* MODIS imager, the L1B calibration accuracy and knowledge of spectral response functions (SRFs) for the 13.6-, 13.9-, and 14.2-μm bands have been improved through comparison with Atmospheric Infrared Sounder (AIRS) spectra. The difference between calculated and observed clear-sky radiances for the CO_2-slicing spectral bands is also mitigated with a

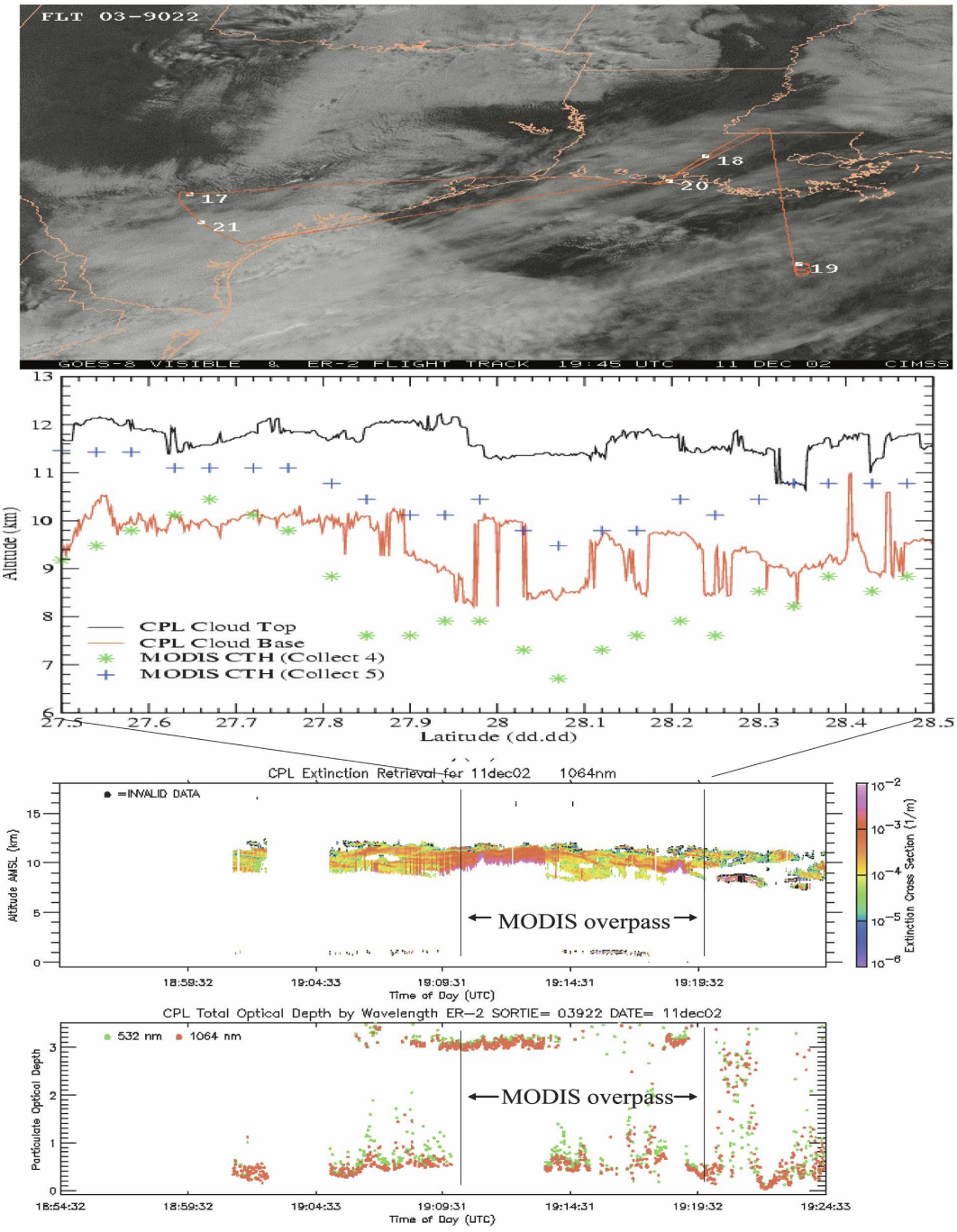

FIG. 3. CPL cloud top and bottom compared with the collection-5 MODIS cloud-top heights (inferred from pressure using the GFS pressure profiles) over cirrus clouds on 11 Dec 2002. (top) ER-2 flight track overlaid on *GOES-8* image, with ER-2 locations indicated in UTC. Segment from 1910 to 1920 UTC coincided with the *Aqua* MODIS overpass. (bottom) CPL altitude and total optical depth determinations from 1854 to 1924 UTC; CPL sees cloud at roughly 10 km, starting with optical depths of about 3 and dropping to 0.5 at 1913 UTC.

radiance bias adjustment. Cloud-top properties are sensitive to the sensor resolution and the sensor view angle. Finally, the cloud retrieval depends on the accuracy of the cloud mask. These considerations are discussed below.

a. MODIS radiance calibration adjustment

As reported in Tobin et al. (2006), comparisons of collocated AIRS and MODIS observations show radiance differences in MODIS CO_2-slicing bands that

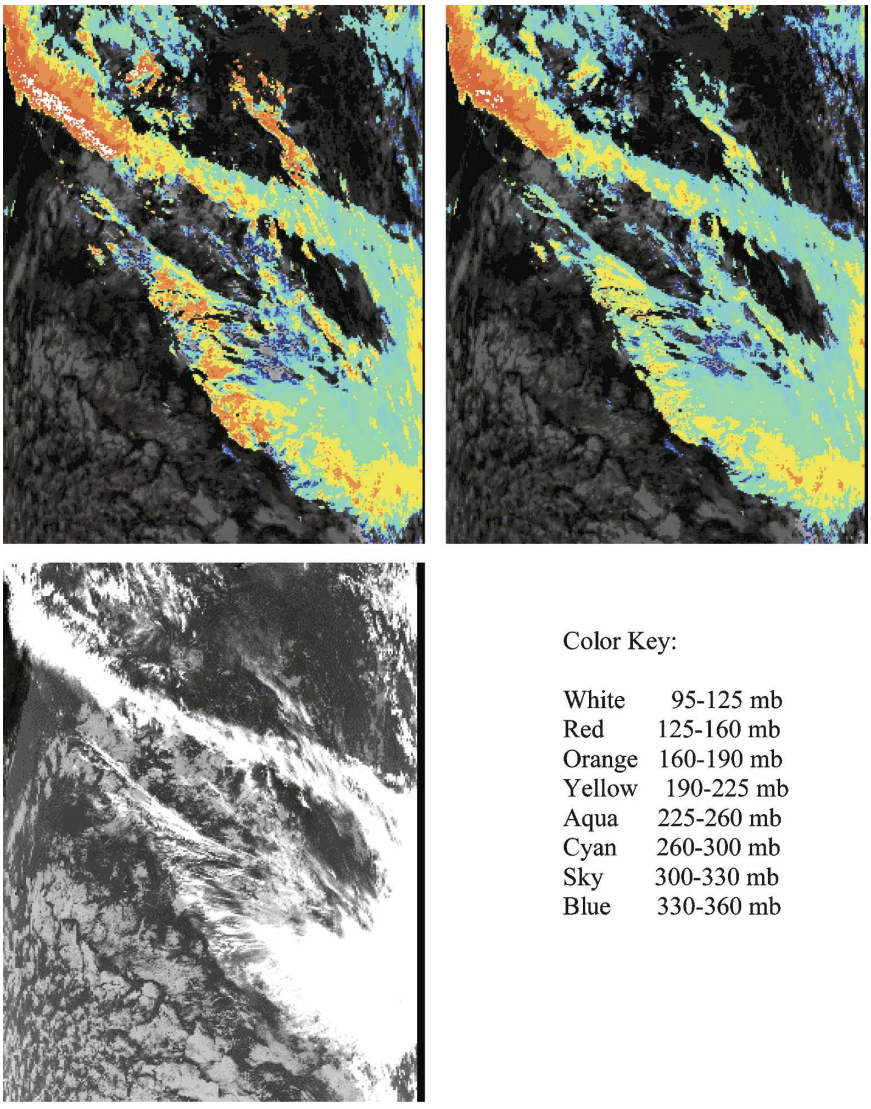

FIG. 4. MODIS granule from 1 Dec 2004 located in the subtropical North Atlantic. (a) Cloud-top pressures using original method of choosing final cloud-top pressure solution (CO_2 radiative error minimization technique), and (b) new results using the top-down method are shown. Only high clouds are shown in colors. (c) Band-31 (11 μm) brightness temperature image.

have significant dependency on scene temperature. This has been corroborated by NASA ER-2 aircraft comparisons with MODIS (Moeller et al. 2006). These radiance differences have been attributed to MODIS cold scene calibration error. The cause of the MODIS radiance calibration errors is undetermined at this time. Tobin et al. show that AIRS and MODIS radiance differences for the same scene are much smaller when the MODIS CO_2 SRFs are shifted slightly (less than 1 cm^{-1}); the scene temperature dependence of the radiance differences is also greatly reduced. However, no physical cause for such a SRF shift has been found. Moreover, subsequent testing with MODIS SRF shifted by the amounts suggested in Tobin et al. has produced nonphysical results in the CO_2-slicing algorithm. Therefore, in collection 5, the radiance differences have been applied to MODIS L1B as a radiance calibration adjustment without modifying the MODIS SRF. For *Aqua*, the adjustments are 0.018, 0.026, and 0.037 W m^{-2} sr^{-1} μm (which are equivalent to 0.25, 0.45, and 0.85 K for typical scene temperatures of 250, 240, and 220 K) for the MODIS 13.6-, 13.9-, and 14.2-μm bands, respectively. For *Terra*, these adjustments are doubled to bring MODIS radiances in line with

TABLE 2. *Aqua* MODIS global cloud-top pressures above 440 hPa (high), between 440 and 700 hPa (middle), and below 700 hPa (low), and clear (IRW optical depth $\tau_{IR} < 0.05$), thin ($\tau_{IR} < 0.7$), thick ($\tau_{IR} > 0.7$), and opaque ($\tau_{IR} > 3.0$) effective emissivities processed at 1, 5, 10, and 20 km for the northern midlatitudes and tropics on 1 December 2004. The MODIS cloud-top properties algorithm relies on the cloud mask at 1-km resolution to determine if a 5-, 10-, or 20-km area is clear or cloudy; this enables MODIS to indicate that low clouds that are thin and thick as well as opaque.

Northern midlatitudes (20°–60°N)					Tropics (20°S–20°N)				
%	Total	Thin	Thick	Opaque	%	Total	Thin	Thick	Opaque
		Resolution: 1 km					Resolution: 1 km		
High	23.2	5.1	12.6	5.5	High	31.3	10.9	12.2	8.2
Middle	17.1	0.3	3.9	12.9	Middle	5.5	0.1	0.9	4.5
Low	31.2	0.0	0.0	31.2	Low	30.2	0.0	0.0	30.2
Clear	28.5				Clear	33.1			
		Resolution: 5 km					Resolution: 5 km		
High	23.7	5.6	13.2	4.9	High	31.9	11.6	13.0	7.3
Middle	17.9	1.5	5.5	10.9	Middle	5.2	0.2	1.0	4.0
Low	39.0	7.1	10.1	21.8	Low	40.2	10.5	10.6	19.1
Clear	19.4				Clear	22.7			
		Resolution: 10 km					Resolution: 10 km		
High	23.7	5.7	13.4	4.6	High	32.7	12.4	13.7	6.6
Middle	17.7	1.7	5.9	10.1	Middle	5.1	0.3	1.1	3.7
Low	40.7	8.3	12.5–19.9		Low	41.7	12.3	12.4	17.0
Clear	17.9				Clear	20.5			
		Resolution: 20 km					Resolution: 20 km		
High	24.3	6.3	13.9	4.1	High	33.5	13.4	14.5	5.6
Middle	18.0	2.0	6.5	9.5	Middle	4.7	0.3	1.0	3.4
Low	42.0	9.5	14.5	18.0	Low	43.4	14.5	14.1	14.8
Clear	15.7				Clear	18.4			

the NASA ER-2 aircraft comparisons in Moeller et al. (2006).

It is important to note that these radiance calibration adjustments do not correct for the differences between observed and model-calculated radiances. Inspection of global fields of observed minus calculated clear-sky radiances exhibit a latitudinal structure, suggesting that a latitudinal clear-sky radiance bias adjustment (possibly indicating temperature dependence in the bias) is needed to mitigate these differences.

b. *Clear-sky-observed versus model-calculated radiance bias adjustment*

Measured and calculated clear-sky radiances differ because of the cumulative effects of instrument noise, spectral response function errors, inadequate knowledge of the atmospheric and surface state, and radiative model approximations. A radiance bias adjustment is necessary to balance the right and left sides of Eq. (3).

A clear-sky 1° latitudinally averaged radiance bias adjustment is created from the 8-day clear-sky radiance bias file. The biases are composited and stored separately by day, night, land, and water for each of the MODIS CO_2 absorption bands. For example, biases from 23 to 30 November 2004, used in processing 1 December 2004, range from -0.1 to $+0.4$ W m^{-2} sr^{-1} μm over land and from -0.05 to $+0.15$ W m^{-2} sr^{-1} μm over oceans. Land values are used for ocean ice cases in the Antarctic region. The precomputed zonal biases, along with the aforementioned radiance calibration adjustments, are added to calculated clear-sky radiances for each CO_2-slicing CTP retrieval.

Figure 2 shows the CTPs before and after application of radiance calibration and bias adjustments for two granules from 1 December 2004. More of the transmissive cirrus is reported as high cloud when the adjustments are applied. Cloud heights are affected more in the middle and high latitudes and less in the deep tropics. On this day, the amount of retrieved high-level transmissive clouds increased by 10% and 13% in the northern and southern midlatitudes, respectively. There was an increase of 11% and 21% additional CO_2-slicing retrievals (as opposed to those from the 11-μm window) in these same regions. The radiance calibration and bias adjustments were tested globally on midwinter, midsummer, and transition season data; in all cases the results were more in family with lidar backscatter and HIRS CO_2-slicing determinations.

The combined effect of the radiance calibration and bias adjustments is further illustrated in Fig. 3 where MODIS cloud-top heights are compared with backscatter data from the Cloud Physics Lidar (CPL; McGill et

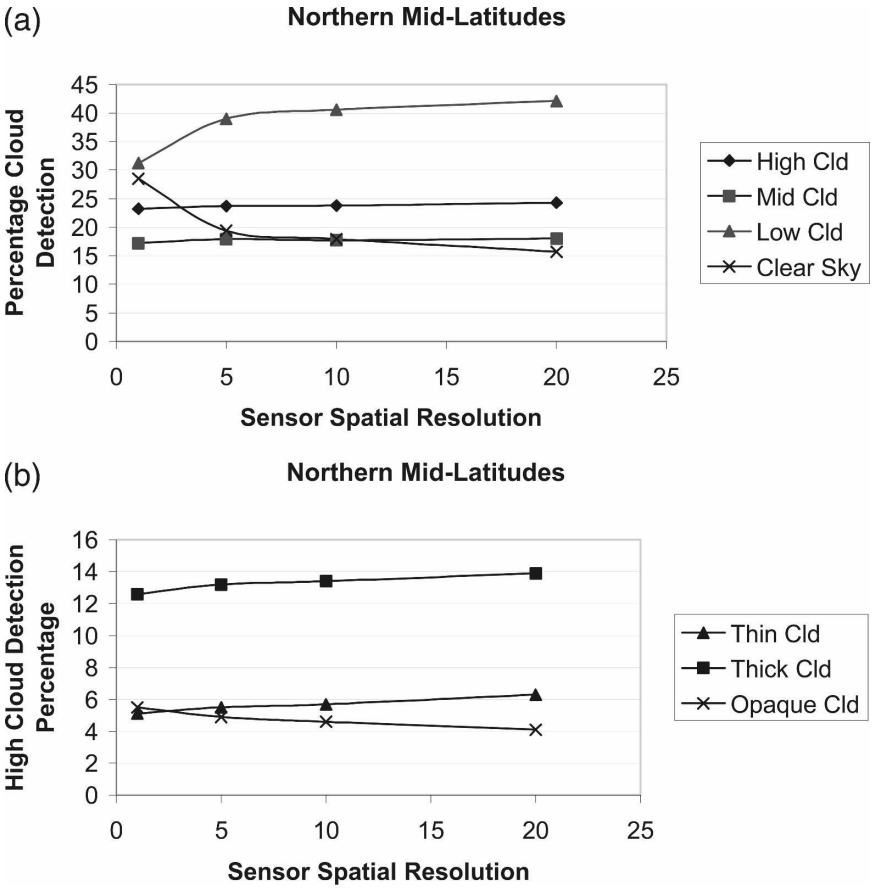

FIG. 5. (a) Frequency of detection of all clouds in northern midlatitudes as a function of sensor spatial resolution on 1 Dec 2004 for *Aqua* MODIS for low (triangles), middle (squares), and high (diamonds) clouds, and (b) frequency of detection of high clouds ($P_c < 440$ hPa) as a function of sensor spatial resolution on 1 Dec 2004 for *Aqua* MODIS for thin (diamonds), thick (squares), and opaque (triangles) clouds.

al. 2002). Neither the radiance calibration adjustment nor the clear-sky radiance bias adjustment was implemented until collection 5; collection 4 is largely the same algorithm except for these considerations. Figure 3 shows that the radiance adjustments used in collection 5 move the cloud-top heights (cloud-top pressures converted to heights using a pressure versus geopotential height profile) from collection 4 up about 3 km; this places collection-5 heights within the cloud extent determined from the CPL, whereas in collection 4 they are well below the cloud base.

c. *"Top-down" versus "CO_2 radiative error minimum" solution approach*

The top-down approach is different from earlier CO_2-slicing approaches. As described in Menzel et al. (1983), cloud-top pressures were previously determined from the various ratios (14.24/13.94 μm, 13.94/13.64 μm, 13.94/13.34 μm, and 13.64/13.34 μm) and the most representative cloud height and amount were those that produced a "radiative error minimum" in the radiative transfer equation calculations for the four CO_2 bands and the infrared window. An example granule using the top-down approach is shown in Fig. 4, along with the CO_2 radiative error minimum approach. The top-down approach shows fewer (presumably) spurious low clouds.

d. *Sensor resolution or field of view*

The results from processing the *Aqua* MODIS global data for 1 December 2004 at various resolutions are found in Table 2 [only the northern midlatitudes (20°–60°N) and tropics (20°S–20°N) are shown for simplicity]. They are separated by cloud type into clear sky (infrared window optical depth $\tau_{IR} < 0.05$), and thin ($\tau_{IR} < 0.7$), thick ($\tau_{IR} > 0.7$), and opaque ($\tau_{IR} > 3.0$)

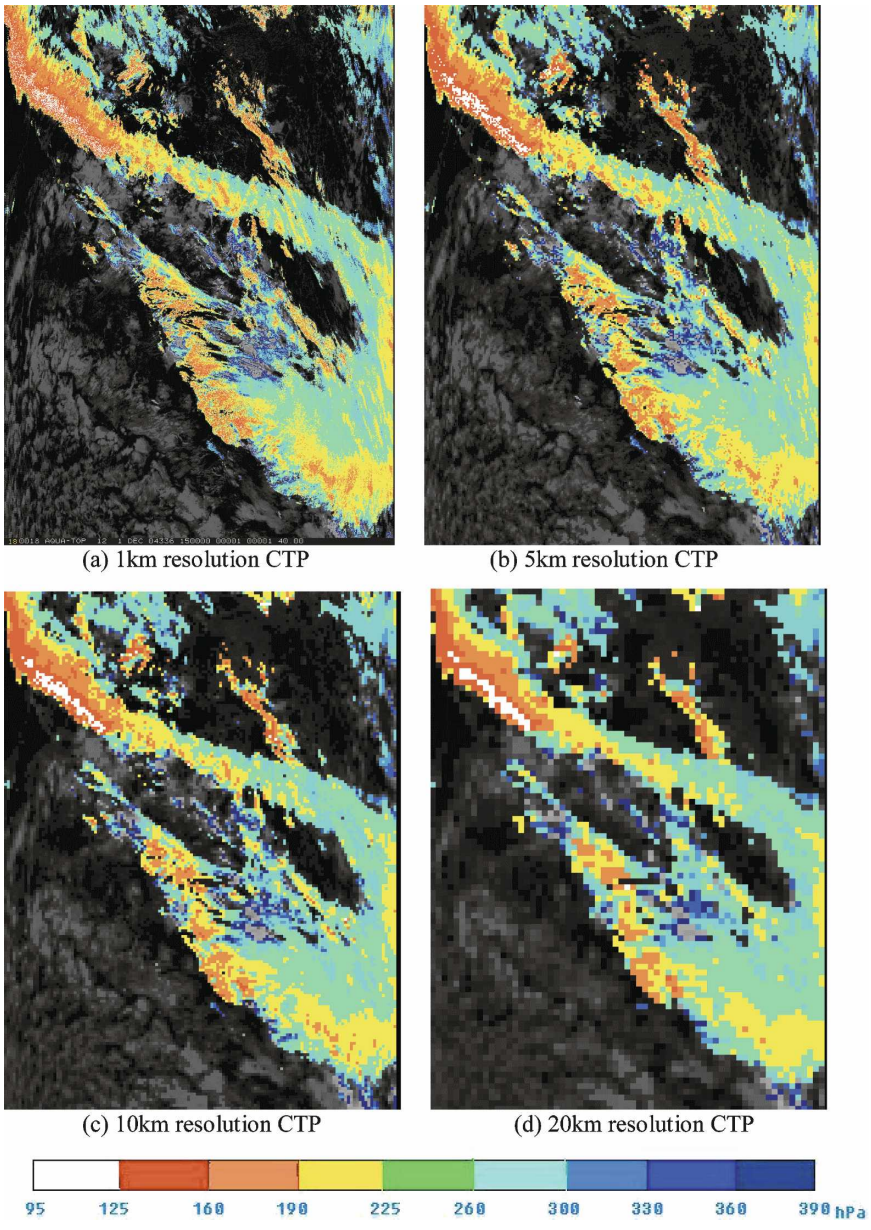

FIG. 6. *Aqua* MODIS high CTP at 1500 UTC 1 Dec 2004 processed at 1- (research MODIS product), 5- (operational MODIS product), 10- (a GOES sounder-like product), and 20-km (a HIRS-like product) resolution.

clouds, and are separated by level in the atmosphere: above 440 hPa (high), between 440 and 700 hPa (middle), and below 700 hPa (low). As might be expected, clear-sky detection falls off with decreasing spatial resolution. At 1 km, clear skies are detected in 28.5% (33.1%) of the fields of view in the northern midlatitudes (tropics); this decreases to 19.4% (22.7%) at 5 km and further drops to 15.7% (18.4%) at 20 km. Most of the decrease in clear sky corresponds to an increase of low clouds. Figure 5 shows a plot of the frequency of detection of clear sky and high-, mid, and low-level clouds in the northern midlatitudes as a function of sensor spatial resolution on 1 December 2004 for *Aqua* MODIS. The largest change occurs moving from 1- to 5-km resolution; from 5 to 20 km there is not much change. For larger target areas, more high, thin and thick (transmissive) clouds are reported but there are less high, opaque clouds. This is presumably due to the observation that opaque portions of cloud systems generally cover a smaller area in a given cloudy region.

TABLE 3. *Aqua* MODIS global cloud-top pressures and effective emissivities processed at 5-km resolution for sensor scan angles less than 18°, between 19° and 32°, between 33° and 41°, and between 42° and 55° for global data on 1 December 2004.

%	Total	Thin	Thick	Opaque
Scan angle: within 18° (−18° ∼ +18°)				
High	20.9	6.2	10.6	4.1
Middle	15.6	0.4	4.9	10.2
Low	36.0	0.0	0.0	36.0
Clear	27.5			
Scan angle: from +18° to +32° and from −18° to −32°				
High	21.3	6.0	11.0	4.3
Middle	16.6	0.3	4.0	12.3
Low	36.9	0.0	0.0	36.9
Clear	25.2			
Scan angle: from +32° to +41° and from −32° to −41°				
High	21.3	5.3	11.2	4.8
Middle	17.8	0.1	2.9	14.8
Low	38.2	0.0	0.0	38.2
Clear	22.7			
Scan angle: from +41° to +50° and from −41° to −50°				
High	21.9	4.7	11.5	5.7
Middle	20.1	0.0	1.5	18.6
Low	39.3	0.0	0.0	39.3
Clear	18.7			
Scan angle: from +50° to +55° and from −50° to −55°				
High	21.9	3.4	11.2	7.3
Middle	23.2	0.0	0.4	22.8
Low	40.4	0.0	0.0	40.4
Clear	14.4			

Figure 6 shows an example of cloud-top pressures at 1-, 5-, 10-, and 20-km resolution for a single MODIS granule. Many finescale details of the cloud pressure field become obvious at 1-km resolution.

e. Sensor viewing angle

The results from processing the *Aqua* MODIS global data for 1 December 2004 at various viewing zenith angles (θ) are found in Table 3. They are separated by viewing angles ($\theta < 18°$, $18° < \theta < 32°$, $32° < \theta < 41°$, $41° < \theta < 50°$, and $50° < \theta < 55°$). Clear-sky detection falls off with increasing viewing angle. Near nadir ($\theta < 18°$), clear skies are detected in 35.6% of the fields of view. This progressively drops to 32.6% ($18° < \theta < 32°$), 29.6% ($32° < \theta < 41°$), 25.2 ($41° < \theta < 50°$), and 21.5% ($50° < \theta < 55°$). This is expected because the sensor field of view increases and the sensor starts viewing clouds more from the edge at increasing slant angles. Figure 7 shows the changes with zenith viewing angle in high, middle, and low cloud detection, as well as high thin, thick, and opaque cloud detection. High cloud detection changes less than 1% over the different viewing zenith angles; a decrease in high, thin cloud detection with increasing viewing angle is compensated by an increase in high, opaque cloud detection. Again, this is thought to be caused by the increased cloud edge viewing at larger angles. Midlevel cloud detection increases the most, going from 14.5% at nadir to 23.9% at maximum viewing angles. This might be the result of increasing viewing angle, enabling the detection of more midlevel clouds that are often obstructed by high clouds (i.e., cloud overlap is decreased by increased sensor scan angle). Low cloud detection increases from 29.3% to 34.3%; this could be due to increased viewing angle, enabling the detection of more low clouds that are otherwise obstructed by high and middle clouds, but also it could be due to more high, thin clouds being incorrectly classified as low, opaque by the infrared window band solution.

Given the changes in cloud detection with viewing zenith angle, a top-down viewing perspective offers less confusion. The approach of Wylie et al. (2005) has been to stay within 18° of nadir for climatological studies.

f. Cloud mask considerations

In the MODIS cloud-top pressure algorithm, initial cloud detection is performed by the MODIS cloud mask (MOD35) algorithm (Ackerman et al. 1998). Global comparisons with the Cloud–Aerosol Lidar and Infrared Pathfinder Satellite Observation (CALIPSO) spaceborne system have shown approximately 85% agreement for both day and night (Holz et al. 2008, manuscript submitted to *J. Geophys. Res.*). Also, for daytime data between February and September 2001, Berendes et al. (2004) report agreement to within ±20% in 77% of cases when *Terra* MODIS is compared to the Vaisala ceilometer that is installed at the Atmospheric Radiation Measurement Program (ARM) site on Alaska's North Slope. Further, they report 81% agreement with the Active Remotely Sensed Clouds Locations (ARSCL) composite laser-derived product, and 74% agreement with the passive Whole-Sky Imager (WSI) from the same site. Because both the ceilometer and WSI are insensitive to optically high, thin clouds, some of the disagreement should not be attributed to MODIS cloud detection errors.

5. Comparison of MODIS cloud-top pressures and amounts with airborne lidar, CALIPSO, and polar-orbiting HIRS

The CO_2-slicing cloud-top pressures have previously been found to be within 50 hPa of lidar (Frey et al. 1999) and geometric determinations (Wylie and Menzel 1989) in situations of single-layer clouds. In multilayer cloud situations, where the upper-layer cloud is semi-

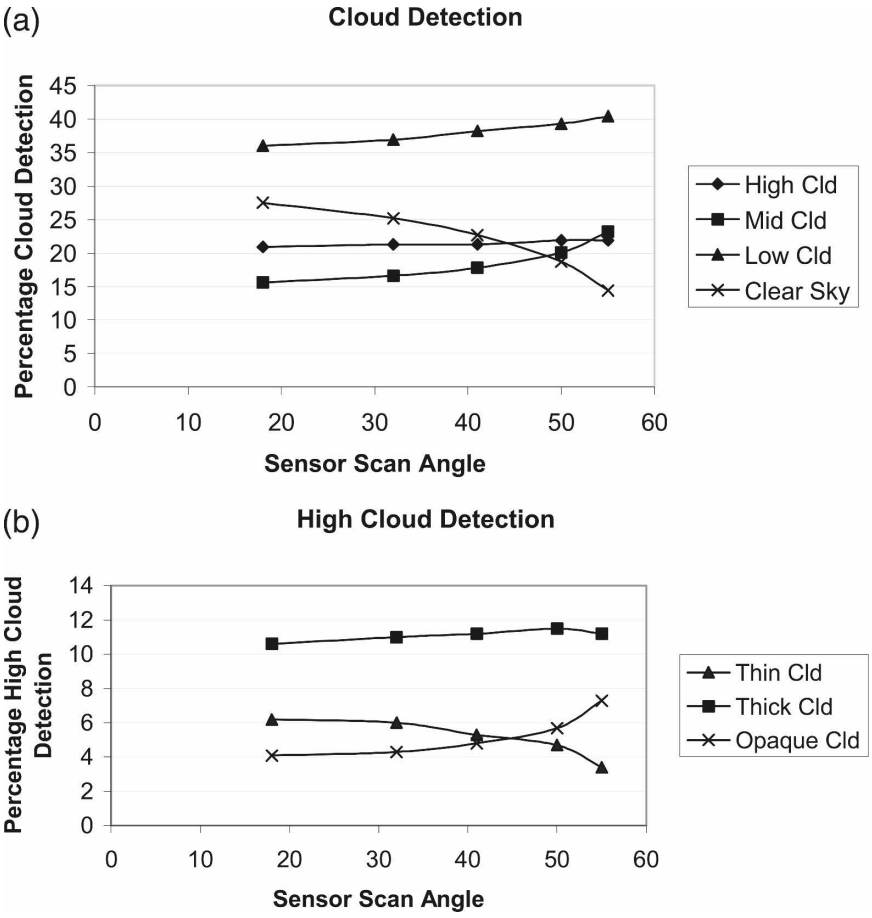

FIG. 7. (a) Detection of high ($P_c < 440$ hPa), middle ($440 < P_c < 700$ hPa), and low ($P_c > 700$ hPa) clouds as a function of sensor viewing angle (less than 18°, 32°, 41°, 50°, and 55°) when processing the MODIS cloud properties at 5-m resolution for the global dataset on 1 Dec 2004, and (b) detection of high, thin, thick, and opaque clouds ($P_c < 440$ hPa) as a function of sensor viewing angle (less than 18°, 32°, 41°, 50°, and 55°) when processing the MODIS cloud properties at 1-km resolution for the global dataset on 1 Dec 2004.

transparent, CO_2 slicing produces a cloud-top pressure representing the radiative mean of the two cloud layers, and hence places the top cloud-layer height between the two layers (Baum and Wielicki 1994). In atmospheres prone to temperature inversions, such as those found in polar regions, the top-down approach places the cloud above the inversion, and hence as much as 200 hPa off its true location. The MODIS cloud property comparisons are in agreement with these earlier assessments of algorithm performance.

a. Comparisons with airborne lidar

For the *Terra–Aqua* Experiment 2002 (TX-2002), a NASA ER-2 aircraft was deployed from 19 November to 12 December 2002 to collect data for validating MODIS and AIRS radiances and cloud products. On each of the ER-2 science missions, the aircraft flew under either *Terra* or *Aqua*, collecting high-spatial-resolution and high-spectral-resolution radiometric data as well as lidar backscatter data. The CPL (McGill et al. 2002) provided cloud and aerosol profiles with 30-m vertical resolution for 200 by 20-m pixels; the CPL depolarization data also provided an indication of cloud thermodynamic phase. Figure 3 shows the comparison of lidar determinations of cloud top and bottom with the collection-5 MODIS cloud-top heights for cirrus clouds observed on 11 December 2002. MODIS cloud-top pressures have been converted to heights using the GFS geopotential height fields. Figure 3 also shows the associated ER-2 flight track overlaid on the *GOES-8* visible image, indicating that the plane was flying northward from 27.5° to 28.5°N under MODIS from 1910 to 1920 UTC. The CPL was viewing ice clouds at 10 km with optical depths of 3 and greater from 1910 to 1913

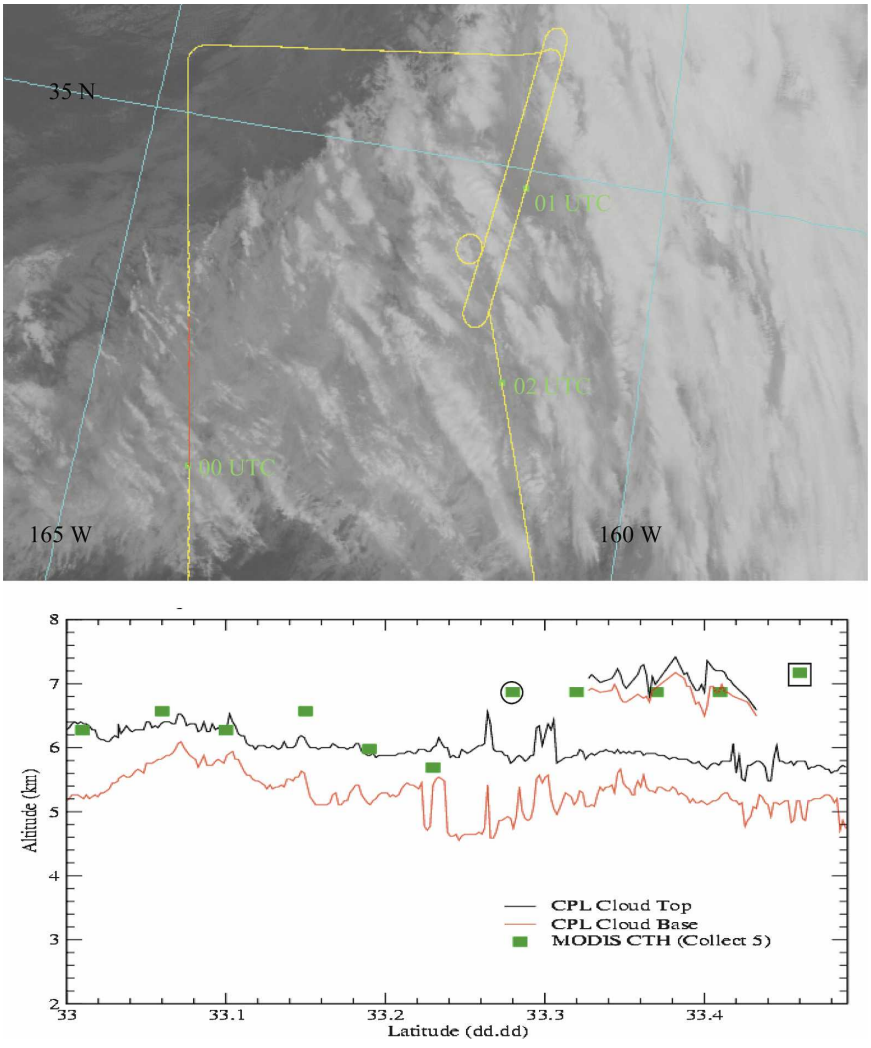

FIG. 8. (top) ER-2 flight track superimposed on MODIS granule; flight tracker from 0005 to 0009 UTC 11 Mar 2003 is shown in red. (bottom) CPL and MODIS collection-5 cloud altitude determinations. MODIS overpass occurred at 0007 UTC. MODIS and CPL see cloud tops around 6 km; MODIS sees the upper clouds at 7 km when two layers are present, beginning at 33.3°N latitude. Circle indicates where CPL narrow-beam nadir view does not see the high clouds seen by the MODIS 5 km × 5 km cloud retrieval. Box indicates where CPL observation time is 2 min after the MODIS overpass and the high cloud seen by MODIS has moved out of the CPL field of view.

UTC, giving way to thin cloud with optical depths of 0.5 after 1913 UTC. MODIS-derived cloud-top pressures are consistently located between the CPL cloud-top and cloud-bottom determinations in these cirrus clouds; this is appropriate, because MODIS is detecting the radiative mean of the cirrus cloud in the CO_2 bands (not the cloud top). Smith and Platt (1978) noted that the difference between the CO_2-slicing-derived pressure and the cloud top is half the cloud thickness for optically thin cloud and less for optically thicker cloud. These results are consistent with that conclusion.

Another comparison over optically thick (optical depths greater than 3) midlevel water clouds from 0005 to 0009 UTC 11 March 2003 is shown in Fig. 8. Again, the comparison is quite favorable (both see clouds at 6 km for most of the scene); however, there are a few locations where disagreements are apparent. In the circled MODIS cloud height at 33.28°N, the CPL narrow-beam nadir pulse misses the high clouds retrieved in the MODIS 5 km × 5 km area. In the boxed MODIS cloud height at 33.46°N, the CPL observation time is 2 min after the MODIS overpass and the high cloud detected by MODIS has moved out of the CPL field of view. Overall, the MODIS cloud heights are within 250

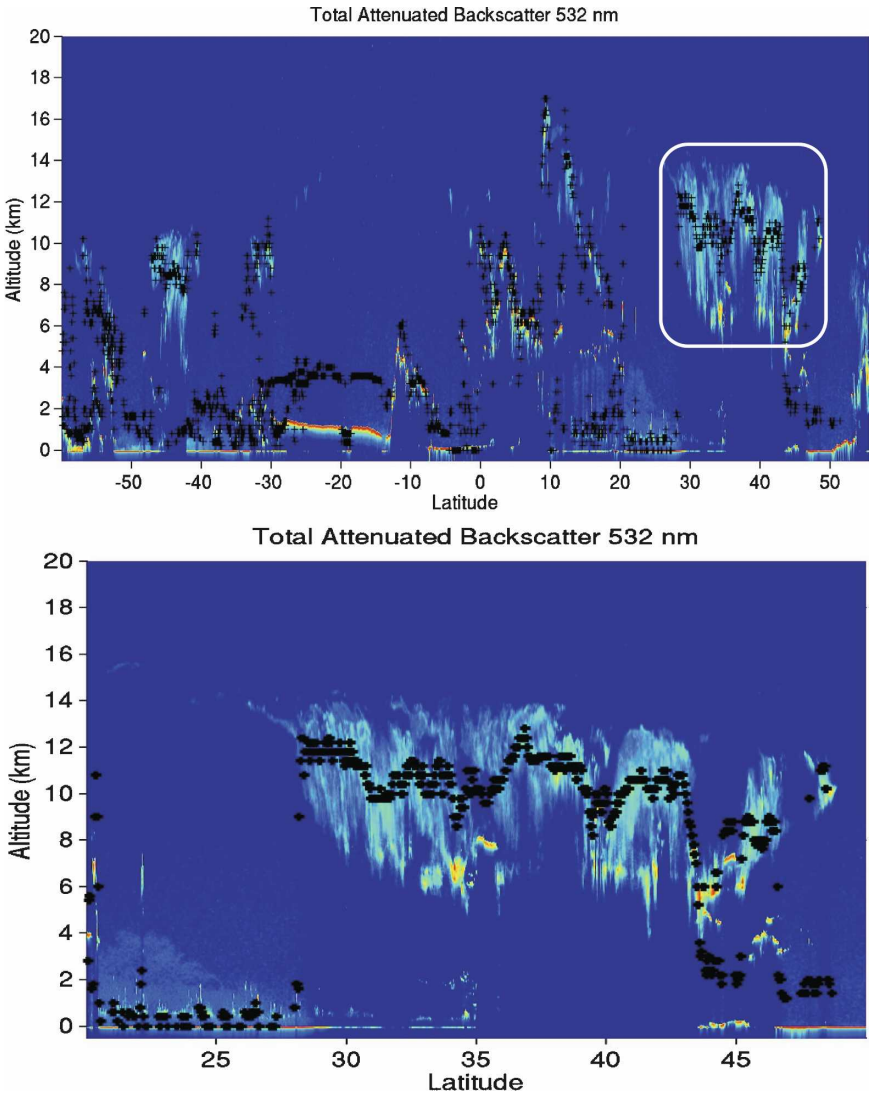

FIG. 9. (top) CALIPSO-attenuated backscatter (at 532 nm) and *Aqua* MODIS cloud-top heights (black pluses) for a flight segment on 15 Jun 2006. (bottom) Zoom on high cirrus at 30°–40°N latitude.

m of the CPL backscatter determinations after the exceptions are understood. The closer agreement between the MODIS and CPL retrievals for water clouds than for cirrus is expected. As measured by the CPL, the liquid water cloud optical thickness becomes very thick (greater than 3) near the cloud top, while the cirrus optical depth is distributed over a large vertical extent. Because the geometric and radiative centers of water clouds are nearly collocated, one would expect close agreement between the CPL and MODIS for these clouds.

b. *Comparisons with CALIPSO*

MODIS cloud property data (found in MOD06 granules) were compared with collocated CALIPSO observations. The CALIPSO instrument takes measurements about 75 s behind that of the *Aqua* MODIS as they both orbit the earth from pole to pole. Collocation is accomplished by matching the CALIPSO latitude and longitude to those of a 5 km ×5 km MODIS cloud-top pressure. Cloud-top pressures were converted to heights using the GFS (as indicted above for airborne lidar comparisons) and were compared to heights from analysis of CALIPSO 0.532-μm backscatter data. An example of comparison for 15 June 2006 is shown in Fig. 9.

High, thin cirrus appears to be estimated very well by the MODIS cloud-top product. Cloud-height differences are mostly within the range expected for visible versus infrared detections. Holz et al. (2006) note that

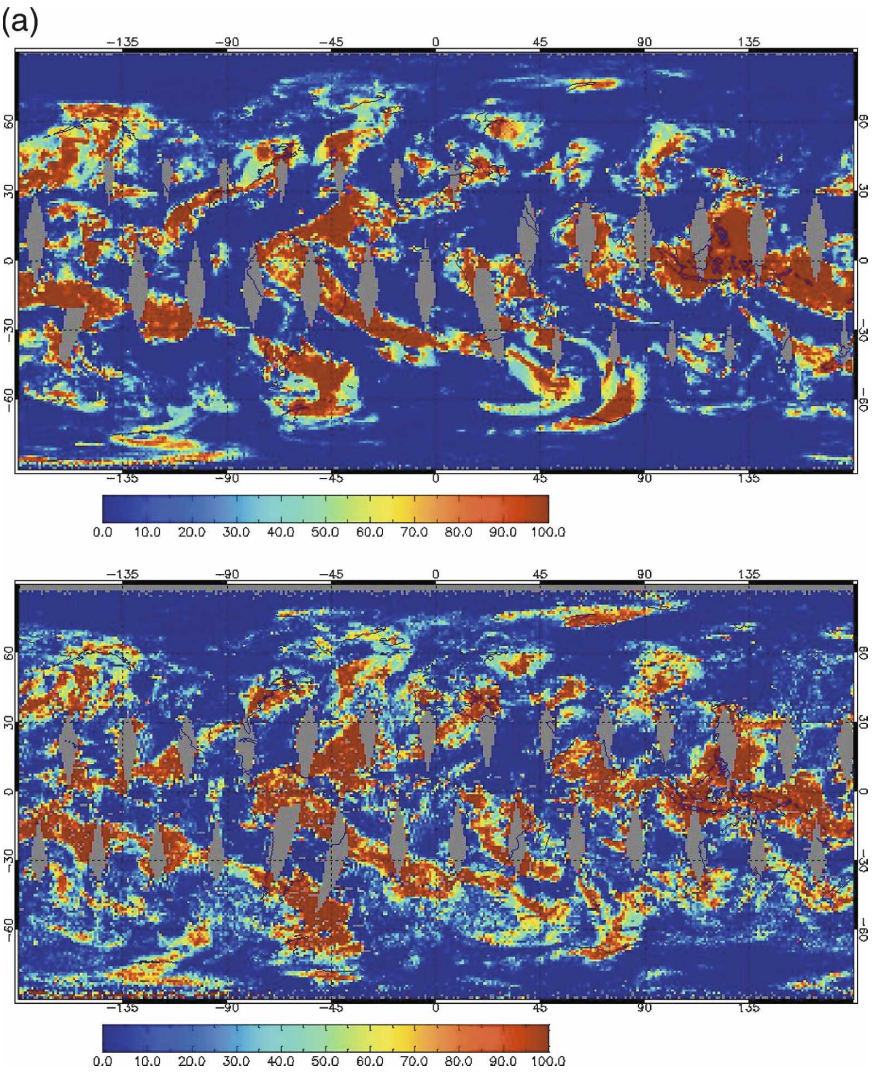

FIG. 10. The 1-day global distributions of (top) *Aqua* MODIS and (bottom) HIRS frequency of (a) high ($P_c < 440$ hPa), (b) middle ($440 < P_c < 700$ hPa), and (c) low ($P_c > 700$ hPa) cloud detection.

geometric differences between the infrared and lidar can be larger then 3 km, but can be explained when considering the integrated optical depth measured by the lidar. The infrared retrieval of cloud-top pressure is possible when the lidar-integrated optical depth is one or higher. For cirrus the geometric depth into the cloud where the optical depth is 1 is frequently over 1 km.

Some large differences are evident at 20°S in low-level clouds where MODIS may be having difficulties caused by the presence of low-level temperature inversions that cause difficulties in cloud-top pressure determination. Widespread and quasi-permanent inversions are found in the eastern portions of oceanic subtropical high pressure regions and in polar night conditions. By using a top-down approach to cloud pressure determination (with the infrared window band), errors in marine stratus regimes (actual minus retrieved) are often positive. A similar algorithm that uses geostationary radiances has errors reported as high as 200–300 hPa (Schreiner et al. 2002). By comparing 11-μm observations to water vapor–corrected Global Data Assimilation System (GDAS) temperature profiles to obtain cloud-top pressures, we are subject not only to measurement errors, radiance modeling errors, and errors resulting from assumptions about cloud coverage and emissivities, but also to errors in the GDAS temperature and relative humidity profiles themselves. Experience has shown that many times in completely cloudy regions a "bottom-up" approach yields the same result as a top-down approach, making a diagnosis of error

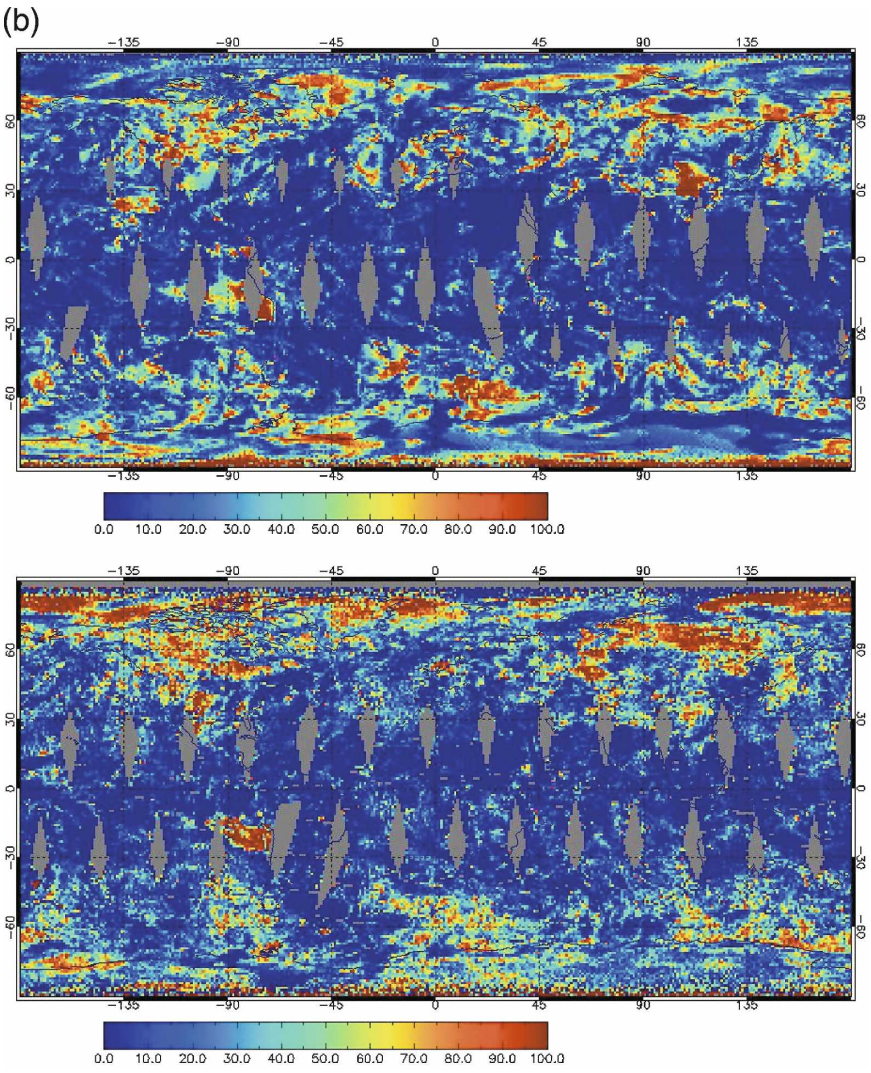

FIG. 10. (*Continued*)

source ambiguous at best. In some other cases, all temperatures in the tropospheric portion of a collocated GDAS profile are colder than cloudy observations, leading to overestimated cloud-top pressures.

The same problems are encountered in areas characterized by polar inversions with the added complications of very cold near-surface temperatures and very deep and sometimes multiple inversions. These effects lead to even smaller signal-to-noise ratios in satellite measurements of low clouds and associated height determinations. Difficulty in discriminating clouds from clear skies is a related issue.

c. Comparisons with HIRS

Figure 10 and Table 4 show the comparison of *National Oceanic and Atmospheric Administration-14* (*NOAA-14*) HIRS and *Aqua* MODIS cloud observations between 60°N and 60°S at 20-km resolution within 45° of nadir for 1 December 2004. The larger scan angle was chosen so that the 1-day coverage of the two instruments in different orbits would be more comparable than 1-day coverage from near-nadir viewing only; thus, the chances of the two instruments seeing different cloud masses would be minimized. The MODIS radiance measurements have been averaged to 20-km resolution. A major remaining difference in the cloud-top properties processing is that the MODIS algorithm relies on the cloud mask at 1-km resolution to determine if a 20-km area is either clear or cloudy, while HIRS investigates cloud presence at 20-km resolution. This enables MODIS to indicate low clouds that are thin and thick, as well as opaque (whereas for HIRS there is no subpixel characterization for low clouds).

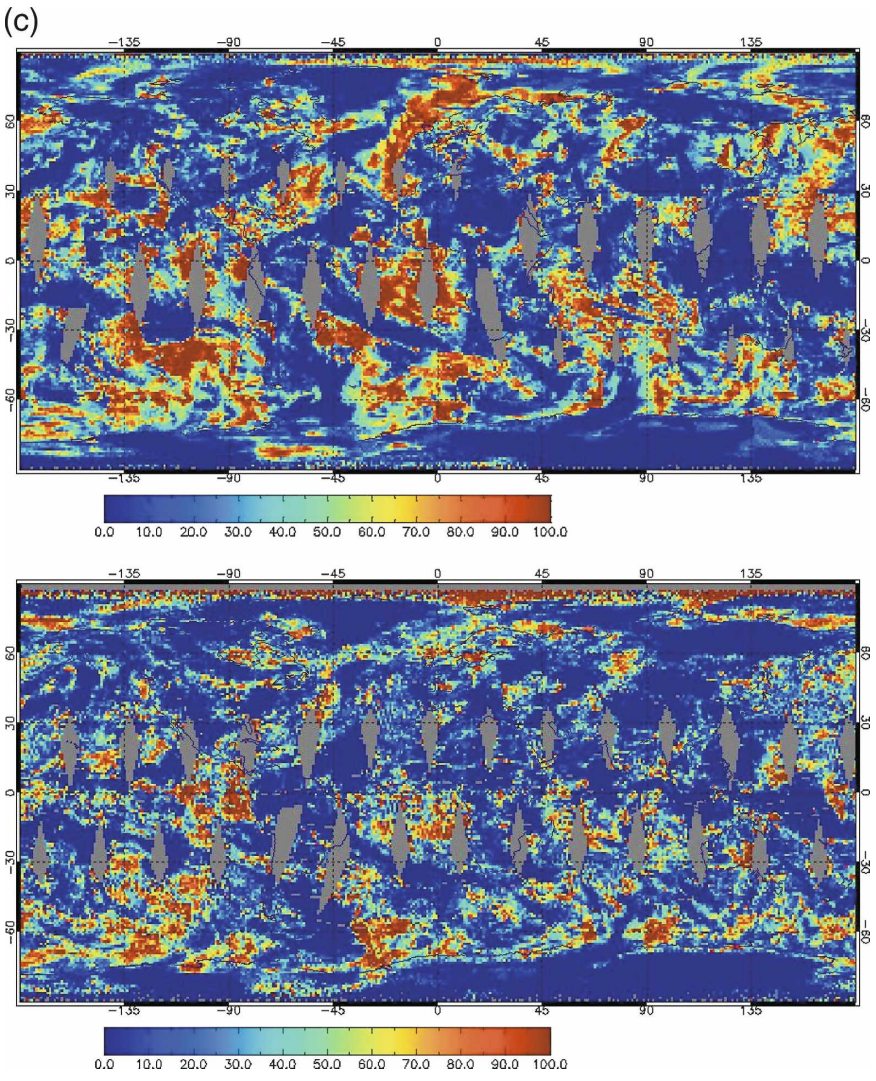

FIG. 10. (*Continued*)

The differences evident in Table 4 are that (a) HIRS and MODIS find cloud cover amounts similar to within 0%–4% in all regions; (b) HIRS finds 2%–4% more high clouds, 2%–4% less middle clouds, and 1%–10% less low clouds than MODIS from 60°N to 20°S; (c) HIRS finds 11% more high, 4% less middle, and 3% less low clouds from 20° to 60°S; (d) HIRS finds 8% more high, thin clouds from 20° to 60°S and 8% fewer middle, thick clouds from 20° to 60°N; and (e) HIRS finds more thin and thick, high clouds and fewer thin and thick, middle clouds everywhere. The differences from 20° to 60°S occur primarily in the southern Indian Ocean.

The frequencies of high cloud detection (Fig. 10a) show very similar global patterns. The frequencies of low cloud detection (Fig. 10c) reveal that MODIS does find more low clouds over the oceans, especially marine stratus near the western continental coastlines. The visible and near-infrared bands used in the cloud mask improve detection of low clouds in MODIS that are unavailable in HIRS. The frequencies of midlevel cloud detection (Fig. 10b) are similar; MODIS is showing more detail in the cloud masses. It is evident that the cloud mask is helping MODIS.

6. Global MODIS cloud-top properties

Level-3 aggregation of cloud properties on a global grid facilitates identification of cloud types (thin, thick, and opaque) and cloud altitude (in 100-hPa segments), and their frequency of occurrence. Histograms of cloud-top temperature and pressure are also available in the level-3 data so that mean, modal, and median products can be determined. Figure 11a shows a global

TABLE 4. HIRS and MODIS cloud observations at 20-km resolution within 45° of nadir from 60°N to 60°S for 1 Dec 2004 for CTP above 440 hPa (high), between 440 and 700 hPa (middle), and below 700 hPa (low), and effective cloud amounts (ECA) classified as thin ($NE < 0.5$), thick ($NE < 0.95$), and opaque ($NE > 0.95$). Percentage of all observations not finding clouds is also indicated as clear. Both HIRS and MODIS algorithms defer to the IRW low cloud detection when the cloud forcing ($R_{clr} - R_{cld}$) is less than 1 mW m^{-2} (sr cm^{-1})$^{-1}$.

	HIRS (scan angle < 45°)				MODIS (scan angle < 45°)				HIRS − MODIS			
	Tot	Thin	Thick	Opaque	Tot	Thin	Thick	Opaque	Tot	Thin	Thick	Opaque
20°–60°N												
High	31.8	13.9	15.1	2.8	27.7	10.2	13.3	4.1	4.2	3.7	1.8	−1.3
Middle	20.5	4.0	5.7	10.8	24.7	7.4	13.6	3.7	−4.2	−3.4	−7.9	7.1
Low	29.9	0.3	1.2	28.4	31.0	10.2	13.2	7.7	−1.1	−9.9	−12.0	20.7
Clear	17.7				16.6				1.1			
20°S–20°N												
High	43.0	22.2	17.1	3.7	40.9	21.2	14.1	5.6	2.1	1.0	3.0	−1.9
Middle	6.8	2.5	2.1	2.3	8.9	4.0	3.7	1.1	−2.1	−1.5	−1.6	1.2
Low	30.7	0.1	0.6	29.9	30.6	13.1	9.8	7.7	0.1	−13.0	−9.2	22.2
Clear	19.5				19.6				−0.1			
20°–60°S												
High	37.8	17.6	17.1	3.1	27.0	9.6	13.0	4.5	10.8	8.0	4.1	−1.4
Middle	15.4	5.0	7.0	3.3	19.4	6.1	10.1	3.2	−4.0	−1.1	−3.1	0.2
Low	36.3	0.2	1.3	34.8	39.4	9.9	16.3	13.2	−3.1	−9.7	−15.0	21.6
Clear	10.5				14.2				−3.7	0.0	0.0	0.0

plot (gridded in 1° latitude × 1° longitude bins) of cloud-top pressures on 1 September 2005, 1 December 2005, 1 March 2006, and 1 June 2006 for *Aqua* MODIS. Coverage gaps in the 1-day global cloud-top pressure product are readily filled with the 8-day global product shown in Fig. 11b.

Table 5 gives the global distribution of cloud pressures (high, middle, and low) and amounts (thin, thick, and opaque) of seasonal means (December–February for boreal winter and June–August for boreal summer) of the *Aqua* MODIS collection 5 from July 2002 to July 2006. Figure 12 shows the corresponding global distribution of cloud-top pressure along with the seasonal difference (shown for daytime only). The major features of the 4-yr MODIS are very similar to those reported elsewhere (Wylie et al. 1994; Wylie et al. 2005). Several common features found in global cloud studies are readily apparent.

The cloud cover follows the sun; latitudinal moisture bands connecting the continents drift north and south with the seasons. There is a preponderance of clouds in the midlatitude storm bands and in the tropics, especially in the Indonesian and west Pacific Ocean warm pool region. This region has year-round high cloud cover (often the global maximum) with values often over 95%. Along with the Indian monsoon, this feature has the most pronounced seasonal oscillation.

Another large seasonal change in cloud cover and height occurs along the intertropical convergence zone (ITCZ) and South Pacific tropical convergence zone. The shift of the ITCZ is pronounced over land, moving from 15°N to 15°S between boreal summer and winter. This large convective development occurs during the austral summer (boreal winter) in South America and Africa, which is readily apparent in the increased detection of cloud, predominately above 500 hPa. This movement of clouds is largely suppressed over the central and eastern Pacific, due to the relatively high heat capacity of the ocean. Subtropical highs just south of the ITCZ in the Pacific and north of the ITCZ in the Atlantic Ocean are relatively cloud free (e.g., near the Bermuda high in summer and the southern Pacific high in December).

In the Northern Hemisphere's midlatitude storm belts, the frequency of clouds increases during the winter with the strengthening of the Aleutian low in the North Pacific Ocean and the Icelandic low in the North Atlantic. The North American cloud cover shows little seasonal change. In the Southern Hemisphere, the eastern Pacific Ocean off South America and the eastern Atlantic Ocean off Africa remain relatively free of clouds throughout the year. The Southern Hemispheric storm belt is evident throughout the year.

Gulf of Mexico moisture intrusion into the southeastern United States, coupled with a summertime convective cloud regime, produces a reduction in cloud cover and a decrease in cloud heights. This is logical because the early afternoon overpass of *Aqua* would allow for the observation of developing, immature cumulus clouds. These clouds would be scattered and generally low in vertical extent.

Little variation is found in the 4-yr average of the

(a)

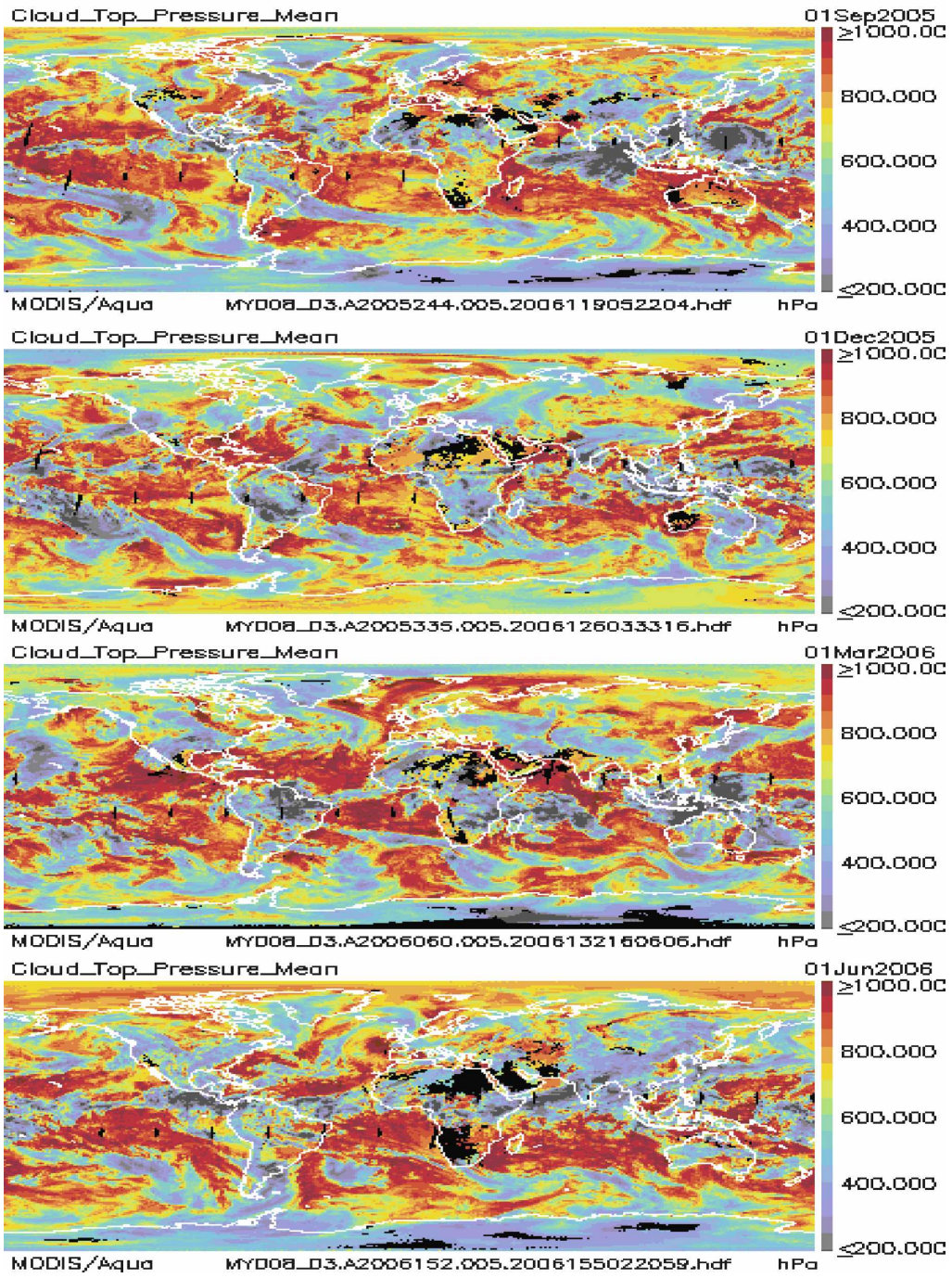

FIG. 11. (a) The 1-day global distributions of *Aqua* MODIS mean cloud-top pressures on 1 Sep 2005, 1 Dec 2005, 1 Mar 2006, and 1 Jun 2006 (online at http://modis-atmos.gsfc.nasa.gov/). Red indicates clear sky; black indicates no CTP retrieval was generated. (b) The 8-day global distributions of *Aqua* MODIS mean cloud-top pressures (hPa; compiled for 1° lat × 1° lon gridded boxes from the previous 8 days) on 1 Sep 2005, 1 Dec 2005, 1 Mar 2006, and 1 Jun 2006 (online at http://modis-atmos.gsfc.nasa.gov/). Red indicates clear sky.

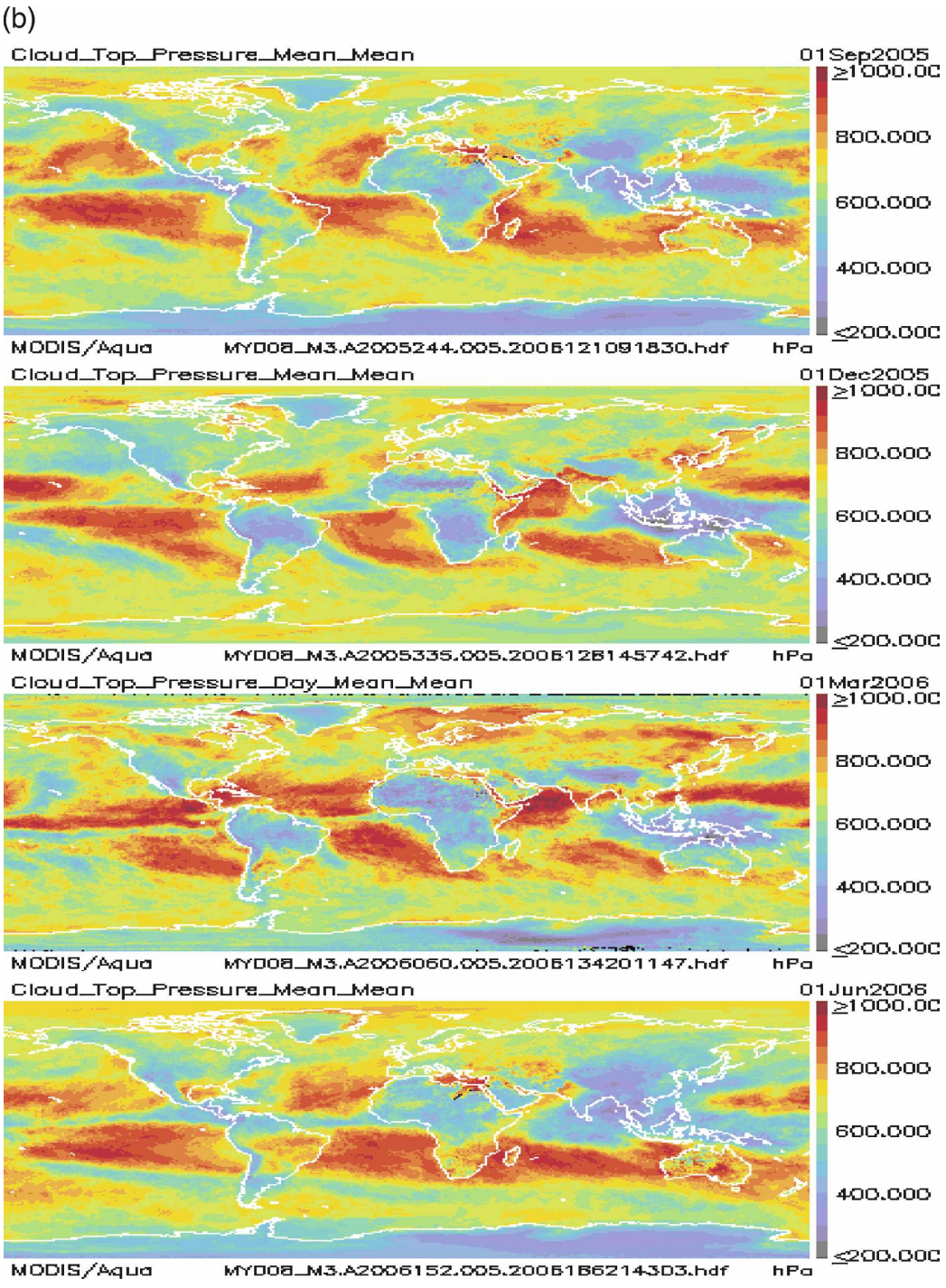

FIG. 11. (*Continued*)

boreal summer versus winter cloud statistics. Clear skies are found in 32.1% of all observations; 1.2% more are found in the boreal summer than in the boreal winter. High clouds (at pressures less than 400 hPa) are evident in 19.51% of the observations; 12.9% of the observations found midlevel clouds (at pressures between 400 and 700 hPa), and 2.5% more are found in winter. Low-level clouds (at pressures greater than 700 hPa) are found in 35.5% of the observations; 1.4% more are found in the summer. Transmissive clouds

TABLE 5. Summer [June–August (JJA)] and winter [December–February (DJF)] percentage of all cloud observations for 2002–06 with CTP above 440 hPa (high), between 440 and 700 hPa (middle), and below 700 hPa (low) and effective cloud amounts (ECA) classified as thin ($NE < 0.5$), thick ($NE < 0.95$), and opaque ($NE > 0.95$). Percentage of all observations not finding clouds is also indicated as clear.

DJF + JJA			ECA		
		0–0.5	0.5–0.95	0.95–1	
	0–400	6.7	11.9	0.9	19.5
CTP	400–700	1.6	5.2	6.1	12.9
	700–1100	8	10.3	17.2	35.5
		16.3	27.4	24.2	
	Clear %	32.1			
DJF only			ECA		
		0–0.5	0.5–0.95	0.95–1	
	0–400	6.7	12	0.8	19.5
CTP	400–700	1.6	5.4	7.1	14.1
	700–1100	7.7	10.1	17	34.8
		16	27.5	24.9	
	Clear %	31.5			
JJA only			ECA		
		0–0.5	0.5–0.95	0.95–1	
	0–400	6.6	11.8	1	19.4
CTP	400–700	1.6	4.9	5.1	11.6
	700–1100	8.3	10.5	17.4	36.2
		16.5	27.2	23.5	
	Clear %	32.7			

(with effective cloud amounts less than 0.95) are found in 43.7% of all observations; this remains about the same for winter and summer.

7. Conclusions

The MODIS cloud-top properties algorithm has become stable in collection 5. Calibrated and navigated MODIS data are processed for 5 × 5 arrays of 1-km pixels. Cloud properties are determined for the cloudy portion of the processing area as indicated by the cloud mask. The data are corrected for satellite viewing angle to minimize the impact of the increased pathlength through the atmosphere of radiation upwelling to the satellite. The algorithm is summarized as follows:

1) Clear minus cloudy radiance differences are determined using the average of the measured cloudy radiances in the 5 × 5 pixel area minus a forward-calculated clear radiance for the CO_2-slicing bands. The NCEP GFS is used to calculate the clear radiances; these forward-calculated radiances must be adjusted for radiance bias (calculated minus measured clear-sky radiance) with respect to clear radiances from the previous 8 days. Possible cloud-top pressure solutions are calculated using the NCEP GFS; this calculation is performed only at the grid spacing of the model.
2) The percent frequency of cloud detection P_c derived from the most opaque bands and the associated window band NE is calculated for the cloudy subset of pixels.
3) Then, NE for the 5 × 5 array is determined from $NE_{5\times5} = N_c(NE/25)$.
4) If cloud forcing is too small (within instrument noise), an infrared window band solution, assuming a low opaque cloud, is used for the cloudy pixels and $NE_{5\times5} = N_c/25$.

Postlaunch characterization of the instrument scan-mirror angle effects as well as cross talk into the long-

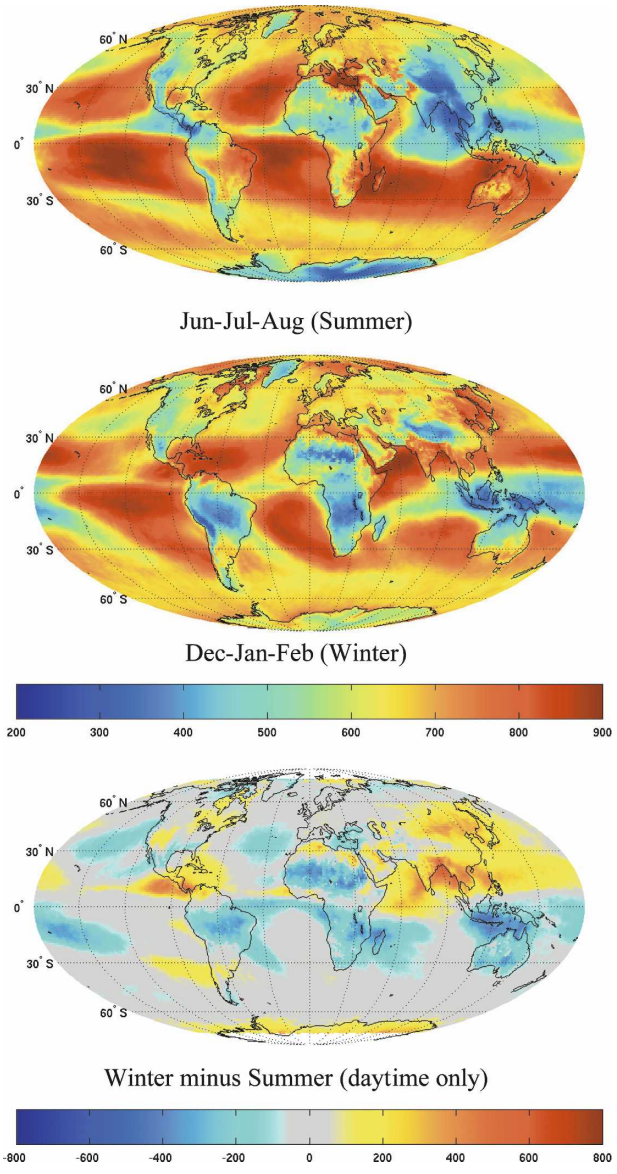

FIG. 12. Seasonal means and differences for *Aqua* MODIS collection-5 cloud-top pressure for 4 yr of data from July 2002 to July 2006: (a) summer (June–August), (b) winter (December–February), and (c) winter minus summer (daytime only).

wave infrared bands has been incorporated into the L1B radiances used in the CTP algorithm. Adjustments for detector striping, radiance calibration, and radiance bias (model-calculated and instrument-measured radiance differences) were found to be necessary and have been successfully made. A top-down algorithm has replaced the radiative error minimum algorithm used previously in CO_2 slicing.

Sensor viewing angle and resolution effects on CTP determinations have been studied and documented. MODIS 5-km-resolution cloud investigations will find roughly 4% more clear skies than HIRS 20-km investigations; most of the difference comes from a decrease of low-level clouds. Near-nadir sensor viewing offers more consistent cloud property estimation; however, restricting MODIS cloud processing to within 18° of nadir assures that more clear 5-km pixels will be found (10% more are found near nadir than at scan angles greater than 41°). Comparisons with airborne and satellite lidar are confirming the validity of the adjusted cloud-top properties algorithm; cloud-top heights are within 1 km (or 50 hPa) in high, optically thin cirrus and midlevel water clouds.

However, in multilayer clouds where the upper-layer cloud is semitransparent, the MODIS cloud pressure represents the radiative mean between the two cloud layers and thus is misleading for the upper-layer cloud-top pressure. Also, in atmospheres prone to temperature inversions, the MODIS cloud algorithm places the cloud above the inversion and hence is as much as 200 hPa off its true location. A two-layer algorithm is under development, and improved performance in the presence of low-level inversions is being studied (a top-down approach could be replaced with a bottom-up approach).

MODIS is starting to generate a cloud dataset that must be understood and connected with the AVHRR and HIRS cloud data; 4-yr indications are that MODIS will be a more-than-worthy successor. The combination of high-spatial-resolution MODIS measurements with high-spectral-resolution measurements from the Advanced Infrared Sounder (AIRS) offers the promise of the best cloud products to date.

Acknowledgments. This work was supported by NASA Contract NNG04HZ39C.

REFERENCES

Ackerman, S. A., K. I. Strabala, W. P. Menzel, R. A. Frey, C. C. Moeller, and L. E. Gumley, 1998: Discriminating clear sky from clouds with MODIS. *J. Geophys. Res.,* **103,** 32 141–32 157.

Baum, B. A., and B. A. Wielicki, 1994: Cirrus cloud retrieval using infrared sounding data: Multilevel cloud errors. *J. Appl. Meteor.,* **33,** 107–117.

Berendes, T. A., D. A. Berendes, R. M. Welch, E. G. Dutton, T. Uttal, and E. E. Clothiaux, 2004: Cloud cover comparisons of the MODIS daytime cloud mask with surface instruments at the North Slope of Alaska ARM site. *IEEE Trans. Geosci. Remote Sens.,* **42,** 2584–2593.

Derber, J. C., D. F. Parrish, and S. J. Lord, 1991: The new global operational analysis system at the National Meteorological Center. *Wea. Forecasting,* **6,** 538–547.

Frey, R. A., B. A. Baum, W. P. Menzel, S. A. Ackerman, C. C. Moeller, and J. D. Spinhirne, 1999: A comparison of cloud top heights computed from airborne lidar and MAS radiance data using CO_2 slicing. *J. Geophys. Res.,* **104,** 24 547–24 555.

Gruber, A., and T. S. Chen, 1988: Diurnal variation of outgoing longwave radiation. *Int. J. Climatol.,* **8,** 1–16.

Hannon, S., L. L. Strow, and W. W. McMillan, 1996: Atmospheric infrared fast transmittance models: A comparison of two approaches. *Proc. Conf. on Optical Spectroscopic Techniques and Instrumentation for Atmospheric and Space Research II,* Denver, CO, SPIE, 94–105.

Holz, R. E., S. Ackerman, P. Antonelli, F. Nagle, R. O. Knuteson, M. McGill, D. L. Hlavka, and W. D. Hart, 2006: An improvement to the high-spectral-resolution CO_2-slicing cloud-top altitude retrieval. *J. Atmos. Oceanic Technol.,* **23,** 653–670.

King, M. D., and Coauthors, 2003: Cloud and aerosol properties, precipitable water, and profiles of temperature and water vapor from MODIS. *IEEE Trans. Geosci. Remote Sens.,* **41,** 442–458.

McGill, M., D. Hlavka, W. Hart, V. S. Scott, J. Spinhirne, and B. Schmid, 2002: Cloud physics lidar: Instrument description and initial measurement results. *Appl. Opt.,* **41,** 3725–3734.

Menzel, W. P., and J. F. W. Purdom, 1994: Introducing GOES-I: The first of a new generation of geostationary operational environmental satellites. *Bull. Amer. Meteor. Soc.,* **75,** 757–781.

——, W. L. Smith, and T. R. Stewart, 1983: Improved cloud motion wind vector and altitude assignment using VAS. *J. Climate Appl. Meteor.,* **22,** 377–384.

——, D. P. Wylie, and K. I. Strabala, 1992: Seasonal and diurnal changes in cirrus clouds as seen in four years of observations with the VAS. *J. Appl. Meteor.,* **31,** 370–385.

Moeller, C. C., H. E. Revercomb, S. A. Ackerman, W. P. Menzel, and R. O. Knuteson, 2003: Evaluation of MODIS thermal IR band L1B radiances during SAFARI 2000. *J. Geophys. Res.,* **108,** 8494, doi:10.1029/2002JD002323.

——, S. Hook, D. Tobin, and V. Walden, 2006: Assessing MODIS LWIR band calibration accuracy. *Earth Observing Systems XI,* J. J. Butler and J. Xiong, Eds., International Society for Optical Engineering (SPIE Proceedings, Vol. 6296), 62960B.

Platnick, S., M. D. King, S. A. Ackerman, W. P. Menzel, B. A. Baum, J. C. Riedi, and R. A. Frey, 2003: The MODIS cloud products: Algorithms and examples from Terra. *IEEE Trans. Geosci. Remote Sens.,* **41,** 459–473.

Reynolds, W. R., and T. M. Smith, 1994: Improved global sea surface temperature analyses using optimum interpolation. *J. Climate,* **7,** 929–948.

Rossow, W. B., and A. A. Lacis, 1990: Global, seasonal cloud variations from satellite radiance measurements. Part II: Cloud properties and radiative effects. *J. Climate,* **3,** 1204–1253.

Schreiner, A. J., T. J. Schmit, and R. M. Aune, 2002: Maritime inversions and the GOES sounder cloud product. *Natl. Wea. Dig.,* **26,** 27–38.

Smith, W. L., and C. M. R. Platt, 1978: Comparison of satellite-deduced cloud heights with indications from radiosonde and ground-based laser measurements. *J. Appl. Meteor.,* **17,** 1796–1802.

Stephens, G. L., 2005: Cloud feedbacks in the climate system: A critical review. *J. Climate,* **18,** 237–273.

Tobin, D. C., H. E. Revercomb, C. C. Moeller, and T. S. Pagano, 2006: Use of atmospheric infrared sounder high-spectral resolution spectra to assess the calibration of moderate resolution imaging spectroradiometer on EOS Aqua. *J. Geophys. Res.,* **111,** D09S05, doi:10.1029/2005JD006095.

Weinreb, M. P., R. Xie, J. H. Lienesch, and D. S. Crosby, 1989: Destriping GOES images by matching empirical distribution functions. *Remote Sens. Environ.,* **29,** 185–195.

Wu, M. L., and J. Susskind, 1990: Outgoing longwave radiation computed from HIRS2/MSU soundings. *J. Geophys. Res.,* **95D,** 7579–7602.

Wylie, D. P., and W. P. Menzel, 1989: Two years of cloud cover statistics using VAS. *J. Climate,* **2,** 380–392.

——, and ——, 1999: Eight years of high cloud statistics using HIRS. *J. Climate,* **12,** 170–184.

——, ——, H. M. Woolf, and K. I. Strabala, 1994: Four years of global cirrus cloud statistics using HIRS. *J. Climate,* **7,** 1972–1986.

——, D. L. Jackson, W. P. Menzel, and J. J. Bates, 2005: Trends in global cloud cover in two decades of HIRS observations. *J. Climate,* **18,** 3021–3031.